SANDIA REPORT SAND85—2843 • Unlimited Release • UC—66
Printed April 1986

FY1984 and FY1985 Geochemistry and Materials Studies in Support of the Magma Energy Extraction Program

H. R. Westrich, L. J. Weirick, R. T. Cygan, M. Reece,
P. F. Hlava, H. W. Stockman, T. M. Gerlach

Prepared by
Sandia National Laboratories
Albuquerque, New Mexico 87185 and Livermore, California 94550
for the United States Department of Energy
under Contract DE-AC04-76DP00789

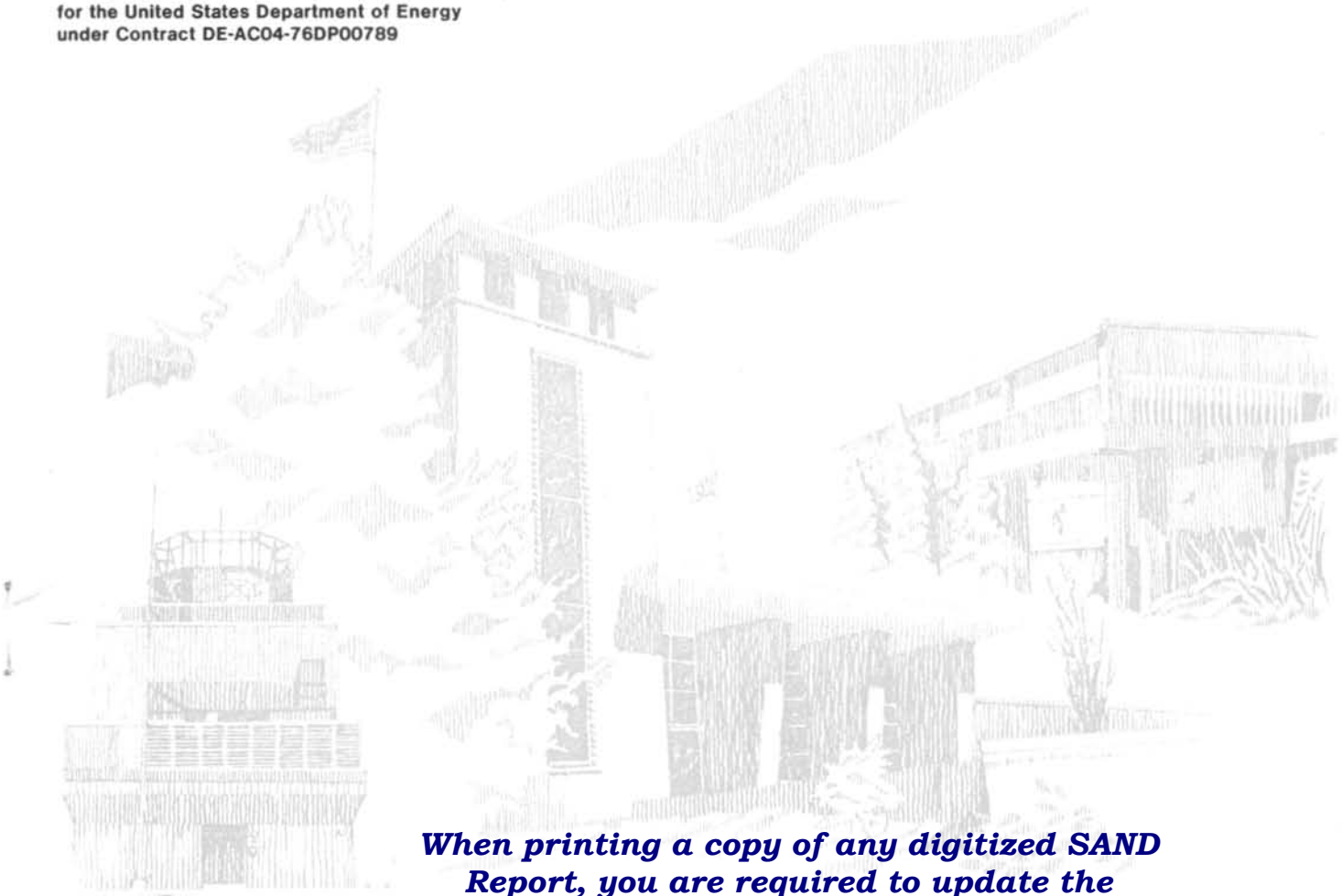

Issued by Sandia National Laboratories, operated for the United States Department of Energy by Sandia Corporation.

Printed in the United States of America
Available from
National Technical Information Service
U.S. Department of Commerce
5285 Port Royal Road
Springfield, VA 22161

NTIS price codes
Printed copy: A04
Microfiche copy: A01

CONTENTS

TABLES

FIGURES

SAND85-2843
Unlimited Release
UC-66

FY1984 and FY1985 Geochemistry and Materials Studies in Support of the Magma Energy Extraction Program*

H. R. Westrich
L. J. Weirick
R. T. Cygan
M. Reece
P. F. Hlava
H. W. Stockman
T. M. Gerlach

Sandia National Laboratories, Albuquerque, NM 87185

ABSTRACT

Geochemistry and materials studies are being performed in support of the Magma Energy Extraction Program. The scope of the studies is dictated by the sites under consideration and the designs of the drilling and energy extraction systems. The work is largely restricted to (1) characterizing magmatic environments at sites of interest, (2) testing engineering materials in laboratory simulated magmatic environments, (3) investigating chemical mass transport effects inherent in designs for direct contact heat exchangers, and (4) evaluating degassing hazards associated with drilling into and extracting energy from shallow magma. Characterizing magmatic environment and testing materials comprised most of the work in FY 1984 and FY 1985, although planning and preliminary experiments in other problem areas were carried out preparatory to fully implementing experimental programs in FY 1986.

Magma characterization studies have been completed for shallow magma at Long Valley, Coso volcanic field, and Kilauea

---

*This work was supported by the U.S. Department of Energy under contract number DE-AC04-76DP00789.

volcano. Procedures have been developed for reconstituting volatiles to experimental rhyolitic magma at concentration levels expected at Long Valley and Coso and for embedding materials in volatile-reconstituted silicate glasses. Experimental facilities and procedures have been developed for subjecting materials to a variety of magmatic conditions ranging from liquidus to subsolidus at pressures up to 200 MPa in the presence of realistic volatile components. The behavior of 17 commercially available materials has been examined in rhyolite magma at 850°C and 200 MPa for periods up to seven days. Preliminary experiments have also been completed on select materials at a range of subsolidus conditions.

Analysis of reaction products from materials tests to date indicate that oxidation is the main corrosion problem for most alloys in rhyolitic magma. Sulfidation is not induced by rhyolitic magma, and reaction with other magmatic components is limited. Grain boundary penetration of materials by oxygen is the principal mode of degradation. The rate-limiting step is mutual volume diffusion of oxygen and metal ions through the oxide reaction rind that develops at the magma-metal interface. Refractory metals and alloys are severely oxidized or recrystallized in rhyolitic magma. Most common austenitic stainless steels show an appreciable penetration of oxygen along grain boundaries. Iron-base, nickel-base, and cobalt-base superalloys show comparatively little grain boundary penetration of oxygen. However, iron-base superalloys have limited strength at magmatic temperatures, and cobalt-base superalloys are prohibitively expensive. Considerations of corrosion resistance, high-temperature strength, and cost indicate nickel-base superalloys offer the most promise as candidates for use in rhyolitic magma. Preliminary results at subsolidus conditions show significantly reduced reaction between metal alloys and silicates compared to that observed in magma and suggest a greatly increased range of feasible materials.

INTRODUCTION

Exploiting the energy potential of magma inevitably entails perturbations of natural and man-made systems. Among the problems raised are, on the one hand, the response of engineering systems to magmatic environments and, on the other, the response of magmatic environments to engineering systems during drilling and energy extraction. The investigation of these problems requires a close collaboration between earth scientists, materials scientists, and specialists in a range of engineering sciences.

The geochemistry and materials studies are constrained by the sites under consideration and the designs of the drilling and energy extraction systems. The sites determine the composition, depth (pressure), temperature, and properties of the magma that are likely to be encountered during drilling and energy extraction and that must be used in laboratory investigations. The designs of the engineering systems enable geochemists and materials scientists to define relevant problems for testing and evaluation.

Most of the geochemistry and materials work centers on the following activities:

1. Characterizing magmatic environments at the sites of interest.
2. Testing materials under conditions expected in magmatic environments.

3. Investigating chemical mass transport effects of direct contact heat exchangers whose operation will involve interactions of fluids with magma and glass-mineral assemblages.
4. Evaluating degassing hazards (vesiculation, outgassing, disruption, and venting) related to drilling into and extracting energy from a volatile-charged silicate melt.

Experimental research in these four problem areas also requires development of techniques for sample preparation, data acquisition, and high-temperature and high-pressure experimentation.

Most of the work summarized below for FY 1984 and FY 1985 dealt with characterizing magmatic environments and testing materials. Planning and preliminary experiments have been carried out, however, for investigations of chemical mass transport effects and degassing hazards. Experimental programs in these areas will become fully implemented in FY 1986.

In addition to the above activities, geochemical studies have also been carried out in support of site selection evaluations. Most of this work was performed in FY 1984 and included field checking and summarizing published data for several potential sites for shallow magma. The results of this work are published elsewhere (Hardee, 1984.)

CHARACTERIZATION STUDIES

Technical Consultants:

H. R. Westrich, 505-846-9613

H. W. Stockman, 505-846-1371

T. M. Gerlach, 505-844-5020

Background

It is essential to characterize the magmatic environments to which engineering materials will be exposed during drilling and energy extraction. The main aspects of the characterization work include the following:

1. The temperatures, pressures, and composition of the magmas at the sites of interest.
2. The petrologic nature of the chillrind that will develop and surround the energy extraction systems.
3. The chemistry of the hydrothermal fluids in geothermal systems above magma at the sites of interest.

The temperatures of shallow rhyolite magma at the higher priority sites of interest (Long Valley, Coso) are expected to lie in the range 700°C to 1000°C. This range is based on data for the melting of granitic rocks (summarized in Burnham, 1979) and estimates from Fe-Ti oxides in the Bishop Tuff (Hildreth, 1979) and the Inyo Dike complex (Vogel et al., 1985) at Long

Valley and in high silica rhyolites at Coso volcanic field (Bacon et al., 1981). At Long Valley, geophysical studies (Sanders and Ryall, 1983; Rundle and Whitcomb, 1984; Rundle et al., 1985) indicate shallow rhyolite magma exists at depths on the order of 5-8 km, which corresponds to pressures approaching 200 MPa. At Coso, depths to magma (5-15 km) may be somewhat greater.

The results of past studies greatly restrict the major element, non-volatile compositions expected for rhyolite magma at Long Valley and Coso. Table 1 summarizes typical or "normal" rhyolite composition ranges based on compilations and summaries taken from the literature (Carmichael et al., 1974; Nockolds et al., 1978). Table 1 also gives anhydrous composition ranges for Long Valley and Coso rhyolites (Hildreth, 1979; Bacon et al., 1981; Stockman et al., 1985).

Because of the importance of magmatic volatiles to the problems of compatibility between engineering materials and magmatic environments, the principal focus of the work to date has been on characterization of the corrosive volatile components (H_2O, CO_2, S, Cl, and F) in magmas at sites currently high in priority (Long Valley, Coso, and Kilauea). This approach was followed in the initial stages of the project, because information is available with which to estimate magma temperatures and pressures, the concentrations of the nonvolatile components, and the compositions of hydrothermal fluids in overlying geothermal systems. The magmatic volatile components (H_2O, CO_2, S, Cl, F), however, are inadequately characterized because of the tendency

Rhyolite Compositions

Wt.% (dry)

Oxide	"Normal"	Long Valley	Coso	Experimental
SiO2	69.0–77.5	69.9–77.4	75.0–77.5	74.02
TiO2	<0.4	<.32	<.10	.28
Al2O3	11.0–15.0	12.3–15.5	12.0–13.0	13.73
Fe2O3*	<4.0	.8–2.7	.8–1.3	1.94
CaO	<2.0	.4–1.7	.3–.5	1.25
MgO	<0.6	<.25	<.02	.25
MnO	<0.1	<.06	<.04	.03
K2O	2.7–6.0	4.4–5.6	4.1–4.8	4.36
Na2O	2.5–5.5	3.3–4.8	3.8–4.6	4.10
P2O5	<0.1	<.06	<.02	.04

* Total iron analyzed in the ferric state

Table 1. "Normal," Long Valley, and Coso rhyolite compositions (wt.%, dry). The experimental composition (experimental) used in the materials tests is for an obsidian from Panum Crater.

of these components to escape during eruption or to be mobilized during crystallization of intrusive magma. In addition to being corrosive, magmatic volatiles are also potentially explosive because of the large volume increases when they exsolve from the magma and form a free gas phase. The solubilities of volatiles in magmatic liquids are poorly known as are the kinetics of vapor bubble nucleation and growth. Hence it is not generally possible, for example, to predict the conditions that could lead to volatile exsolution and large volume increases during drilling into magma. However, for this problem to be examined experimentally, the concentrations of volatiles dissolved in the magma at depth need to be known.

Two approaches are being used to characterize magmatic volatiles at potential sites for the Magma Energy Extraction Program. One is to sample volatiles directly from fumaroles (e.g., Gerlach and Graeber, 1985). The other is to measure the volatile contents of glassy volcanic ejecta (obsidian), which forms when rhyolite magma quenches during eruption and retains its initial dissolved volatiles (Eichelberger and Westrich, 1981; Westrich et al., 1985). The latter method is particularly well suited for the volatile characterization of rhyolitic magma, which is of primary interest to the current project.

FY 1984 Activities

Several analytical techniques and procedures were evaluated and developed for bulk analyses of H_2O, CO_2, S, Cl, and F in obsidian glasses. Existing H_2O analytical techniques using Karl Fischer titration were refined. Water evolution from obsidian was achieved by simple pyrolysis of sieved fragments, eliminating the need for flux fusion. A CO_2 determination procedure was developed that is based on infrared absorption. Enhanced X-ray fluorescence (XRF) spectroscopy techniques were developed for Cl and S analyses. A specific ion electrode technique was employed for F analysis of obsidian. All techniques were tested against natural and synthetic standards, including USGS standard rocks. Although further development of analytical techniques will continue as needed, the techniques and procedures now in hand appear to be satisfactory for future bulk volatile characterization required by the project.

The accuracy of S analyses for silicate glasss is especially crucial in materials testing becuase of potential metal sulfidation problems. Conventional XRF analysis for sulfur in obsidian was improved by employing synthetic sulfur standards (rock matrix plus added FeS_2, $BaSO_4$, or $NaSO_4$ solution) in addition to USGS rock standards. Calibration curves for the synthetic standards proved to be highly linear and reproducible; the machine blank was reduced to < 5 ppm, allowing for S determinations down to 5-10 ppm. Special washing procedures were also developed to remove

sulfate (and chloride) incrustations in vesicles of some obsidians that gave anomalously high S contents.

Recent blade cuts for drilling pads and a power plant site at the Coso KGRA (Known Geothermal Resource Area) have exposed several airfall strata formed during the most recent eruptions at Coso and provided an opportunity to collect fresh, rapidly cooled, obsidian samples containing trapped magmatic H_2O, S, Cl, and F. Reconnaisance sampling of the airfall units was undertaken and laboratory analysis of volatiles in the quenched rhyolitic liquids was initiated. Similar studies on obsidian airfall from the recent rhyolite eruptions in the Long Valley-Mono Lake region were also pursued. The results of these investigations are presented below with the FY85 results.

Gas samples were collected and analyzed from the current 1983-1986 east rift eruption of Kilauea Volcano and from the 1984 eruption of Mauna Loa Volcano. This work, funded by the DOE/OBES/Geosciences Magma-Hydrothermal Project, is relevant to the Magma Energy Program. These analyses provided the first reliable analyses for halogens (HCl, HF) in basaltic gases. Samples of rapidly quenched glass from fire fountains were also collected and analyzed for H_2O, CO_2, S, Cl, and F. These results permitted definition of the volatile concentrations for magma in the east rift reservoirs of Kilauea (Gerlach and Graeber, 1985). Volatile concentrations are currently better understood for Kilauea magma than for magma at any other site under consideration. Fumarole gas sampling has also been initiated

under DOE/OBES funding at Long Valley and the Coso volcanic field.

FY 1985 Activities

The volatile concentrations of magmas at the sites of interest are shown in Table 2. The ranges shown for Long Valley and Coso rhyolite are based on approximately a hundred analyses performed at Sandia Labs. (Westrich et al., 1985; Westrich, unpublished data) supplemented with some published data for F (Hildreth, 1979; Bacon et al., 1981). Minor differences in magmatic volatile content exist between the Coso and Long Valley magmas. The lower water contents observed for Coso obsidian probably reflects inadequate sampling of early, more volatile-rich tephra units, while the higher F contents appear to be significant. The Kilauea volatile concentrations are based on the work by Gerlach and Graeber (1985). The differences between rhyolitic and basaltic magmatic volatiles are significant and could pose different material compatibility problems.

Preliminary characterization has been completed on the chillrind expected to form adjacent to a closed system heat exchanger. Heat transfer calculations for a closed system heat exchanger operating at 500°C in 850°C rhyolite magma indicate initial cooling rates for near-field magma (within 0.2 m of the heat exchanger) of 125°-150°C/hr and approximately 5°/hr for far-field magma (about 0.4 m from the heat exchanger). With time,

Magmatic Volatile Concentrations

Magma Source	H2O wt.%	F ppm	Cl ppm	S ppm	CO2 ppm
Long Valley	<3.0	500–800	435–580	20–65	<10
Coso	<1.5	1100–1800	725–890	25–55	<10
Kilauea	<0.3	400	90	700	350.
Expt (unsat)*	3.0	725	700	40	<10
Expt (sat)*	>6.0	900	910	60	<10

* Volatile saturated or undersaturated experiments

Table 2. Volatile concentrations in magmas fro sites of interest and volatile-reconstituted rhyolites (experimental) used in materials tests; saturated (sat) and undersaturated (unsat) refer to the presence or absence of a fluid phase.

both the rind thickness and local cooling rates will change. Cooling experiments for simulated near-field magma at 200 MPa produced 100% glass; preliminary results for far-field cooling of magma show assemblages containing 65% glass and 35% crystals (magnetite, biotite, and feldspar?). Intermediate cooling rates of 40°-60°C/hr produce 80% glass and 20% crystals (magnetite and biotite).

COMPATIBILITY STUDIES

Technical Consultants:

H. R. Westrich, 505-846-9613

L. J. Weirick, 505-844-1016

R. T. Cygan, 505-844-7146

M. Reece, 505-846-4389

P. F. Hlava, 505-844-6174

Background

Engineering materials must be found that will survive high temperatures and pressures as well as the corrosive nature of magmatic liquids. The survivability of pure metals in basalt buffered by C-O-H-S gas typical of basaltic lava was investigated at 0.1 MPa during the DOE/OBES Magma Energy Project (Douglass and Healey, 1979; Douglass and Ehrlich, 1982; Douglass, 1983). These early studies showed that sulfidation was the main corrosion problem for materials in basaltic magma at low pressure. Investigations were not performed at high pressure nor were they carried out in the more siliceous (rhyolitic) magmas expected in the shallow crust of the western U.S. The volatiles in a rhyolitic magma are substantially different from a basaltic one (see Table 2). There is, therefore, a need for an experimental program that will address the problems of materials compatibility in simulated, high-pressure silicic magmatic environments with appropriately reconstituted volatiles.

FY 1984 Activities

The main emphasis of the FY 1984 work was on planning FY 1985 experiments, developing experimental procedures required by the plan, and performing preliminary tests.

A detailed experimental plan was formulated for investigating the compatibility of numerous commercial metals in simulated magmatic environments. The plan calls for fully simulated rhyolite magmatic environments in the 3-8 km depth range (100-200 MPa) at temperatures up to 850°C with reconstituted volatiles (Table 2). Several environments ranging from the chillrind surrounding a closed heat exchanger outward to the magma body itself were specified for testing of alloys. The environments include (1) the 850°C volatile-bearing rhyolite magma at 200 MPa (to test alloy response to magma in the event of a loss-of-cooling accident); (2) the 500°C volatile-bearing glass chillrind quenched at 100-200 MPa around a heat exchanger (to test alloy response to an expected normal operating environment); and (3) the 500-700°C, 50 MPa hydrothermal fluids expected in the fractured and crystallizing chillrind (to test material response to fluids permeating the silicate rubble adjacent to the heat exchanger). The volatile concentrations chosen for the synthetically prepared experimental magmas and glasses are based on the Long Valley and Coso volatile data and water solubility estimates (Table 2).

1. Selection of rhyolite for tests

Major element, non-volatile compositions for rhyolite are relatively restricted, as noted above and shown in Table 1. Obsidian from Panum Crater near Mono Lake, California, provides the experimental rhyolite for the compatibility tests. The composition of this glass (without volatiles) lies between that of the Long Valley and Coso rhyolites and is representative of most rhyolites. Volatiles are restored to the Panum Crater obsidian by procedures described below. The volatile concentrations of the reconstituted experimental rhyolite are given in Table 2 for saturated and undersaturated conditions and should be representative of pre-eruptive rhyolitic magma.

2. Selection of materials for tests

Table 3 lists the 17 commercially available materials selected for the magma energy compatibility tests. The list includes a representative from each family of materials typically used for its chemical resistance in high-temperature environments. In general, these materials are listed in order of increasing alloy complexity, including the number of components, fabricability, weldability and availability, and increasing chemical resistance, mechanical strength and cost. For the iron-, nickel-, and cobalt-base alloys, the chromium content is at least 15% (by weight), which is the minimum required for formation of a protective chromia film in an oxidizing environment.

Magma Energy Compatibility Test Materials

NAME	COMPOSITION (wt.%)						
	Fe	Cr	Mn	Ni	Co	Mo	Others
Carbon Steel							
1095	97.9	--	0.5	--	--	--	0.2 Si, 1.0 C (est.)
Stainless Steel							
304 (Austenitic)	71.9	18.0	0.6	8.5	0.2	0.1	0.3 Si
26-1 (Ferritic)	70.5	27.6	--	0.1	--	1.0	0.3 Si, 0.1 Nb
310 (Austenitic)	51.4	25.1	1.6	19.6	0.3	0.3	0.6 Si
Superalloys							
RA330 (Fe-base)	38.0	18.9	5.0	35.2	0.1	0.1	0.9 Si
20Cb-3 (Fe-base)	40.1	19.0	0.4	33.3	0.1	2.2	3.0 Cu, 0.5 Si, 0.5 Nb
Inconel 625 (Ni-base)	2.1	21.1	--	63.3	--	9.0	3.9 Nb, 0.3 Ti, 0.2 Al
Inconel 718 (Ni-base)	15.9	18.6	--	55.1	--	3.0	5.4 Nb, 1.0 Ti, 0.7 Al
Eigiloy (Co-base)	13.9	20.1	2.0	15.5	40.0	7.3	0.9 Si
Alumina/Chromia Formers							
Kanthal A-1 (Fe-base)	72.3	20.6	0.1	0.3	0.1	--	5.9 Al, 0.5 Si
Nimonic 105 (Ni-base)	0.5	14.4	0.1	54.4	19.5	5.1	5.4 Al, 1.3 Ti, 0.2 Si
Cabot 214 (Ni-base)	2.5	15.2	0.2	76.9	--	--	5.0 Al
	Ti	Mo	Zr	Sn	Ta	Re	Others
Alloys/Refractory Metals							
Mo	--	99.9	--	--	--	--	
Re	--	--	--	--	--	99.9	
T-111	--	--	--	--	89.7	--	8.8 W, 1.9 Hf
Ti-Code 12	97.0	--	--	--	--	--	3.0 Cu
Zircalloy-2	--	--	98.3	1.5	--	--	0.2 Fe, 0.1 Cr

Table 3. Microprobe analyses of commercially available metals used in compatibility tests.

The 1095 carbon steel was selected to be a representative for the API Grade steels such as H-40, K or J-55 and N-80, which are high carbon steels commonly used as drill stem and casing. 304 stainless steel was selected from the austenitic stainless steel family because of its popularity. 310 is a more highly-alloyed austenitic stainless steel used in environments demanding improved chemical resistance and strength beyond 304 SS. 26-1 is a high-purity, ferritic stainless steel containing no nickel and very low levels of carbon and nitrogen. Unlike austenitic stainless steels, 26-1 is immune to chloride stress cracking. RA-330 was chosen as the representative for the iron-base superalloy family. It contains small amounts of silicon, which imparts an added chemical resistance due to the formation of a silica film in an oxidizing environment. The 20Cb-3 test materials is another iron-base superalloy which has an addition of copper for increased stress corrosion cracking resistance and molybdenum for pitting resistance in predominantly aqueous chloride environments.

Inconel 625 is a desirable choice in the solution-hardened, nickel-base superalloy family. It has excellent chemical resistance, is virtually immune to stress corrosion cracking and has excellent high-temperature strength. Inconel 718 improves upon Inconel 625 with higher strength at high temperatures due to its precipitation hardening characteristic. However, it is more difficult to fabricate and weld than Inconel 625. Elgiloy is a generic representative for the cobalt-base superalloy family.

Figure 1 compares the tensile strengths of carbon, stainless, and superalloy materials by alloy family at 850°C. The tensile strength, or ultimate tensile strength (UTS), is the ratio of the maximum load to the original cross-sectional area of the specimen. The tensile strength is the value most often quoted from the results of a tension test. For ductile metals the tensile strength should be regarded as a measure of the maximum load which the material can withstand under the very restrictive conditions of uniaxial loading. In general, strength decreases and ductility increases as the test temperature is increased. As mentioned previously, as the alloy complexity increases from simple carbon steels through iron-base, nickel-base and then cobalt-base alloys, the strength at high temperatures improves dramatically.

The creep-rupture strength of these materials after 100 hours at 850°C (Figure 2) is analogous to their tensile strength. The basic information obtained from a stress-rupture test is the time to cause failure at a given nominal stress for a constant temperature. After a series of these tests are made, it is possible to extract the stress level which will cause the metal to fail at a given test time, such as 100 hours. Thus the strength and stability of a material relative to other materials at an elevated temperature can be represented by creep-rupture strengths.

Unfortunately, cost also follows the same pattern as shown in Figure 3. Although cobalt-base alloys have the best strength,

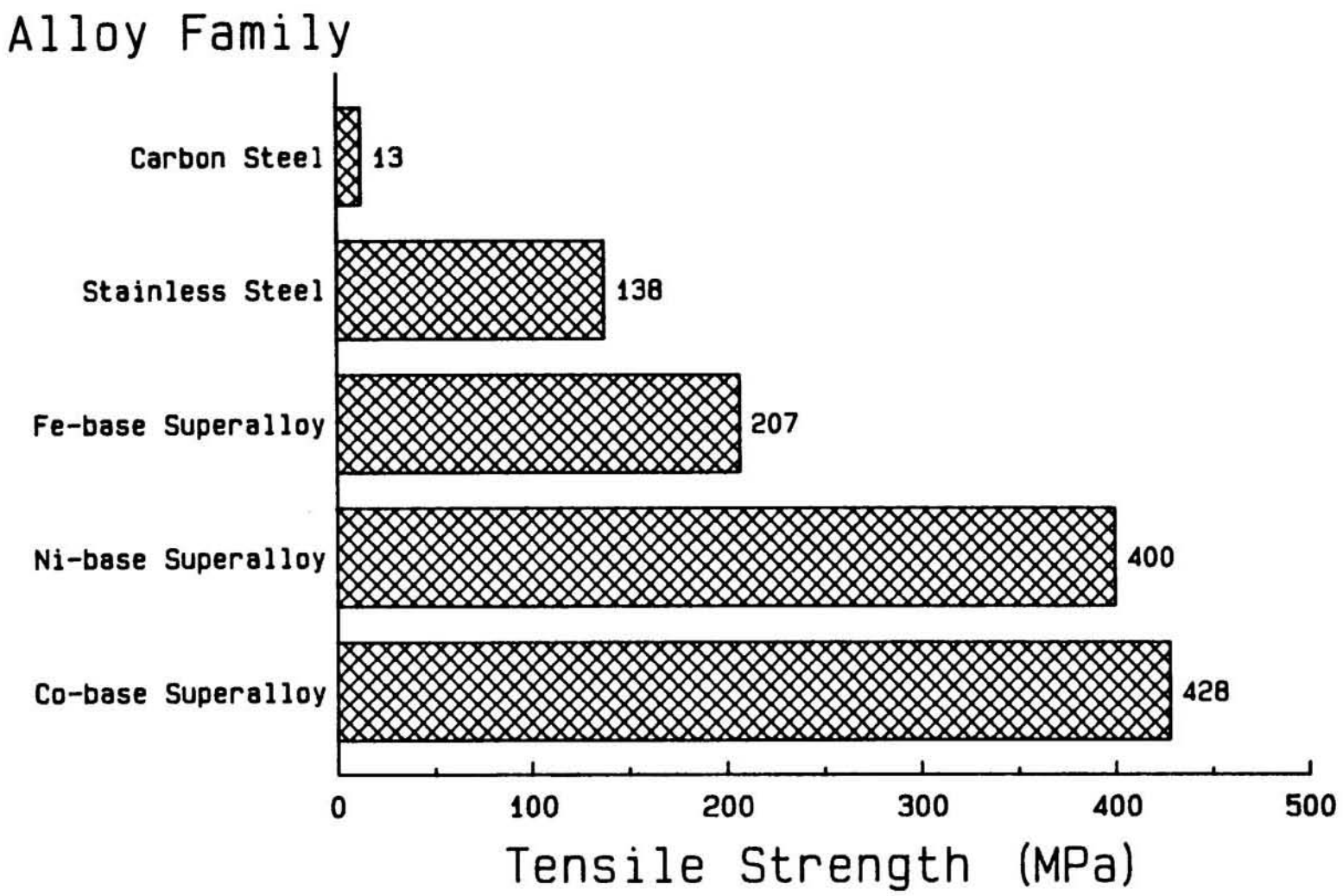

Figure 1. Tensile strengths (MPa) of alloy families at 850°C (ASM Metals Handbook, 1978).

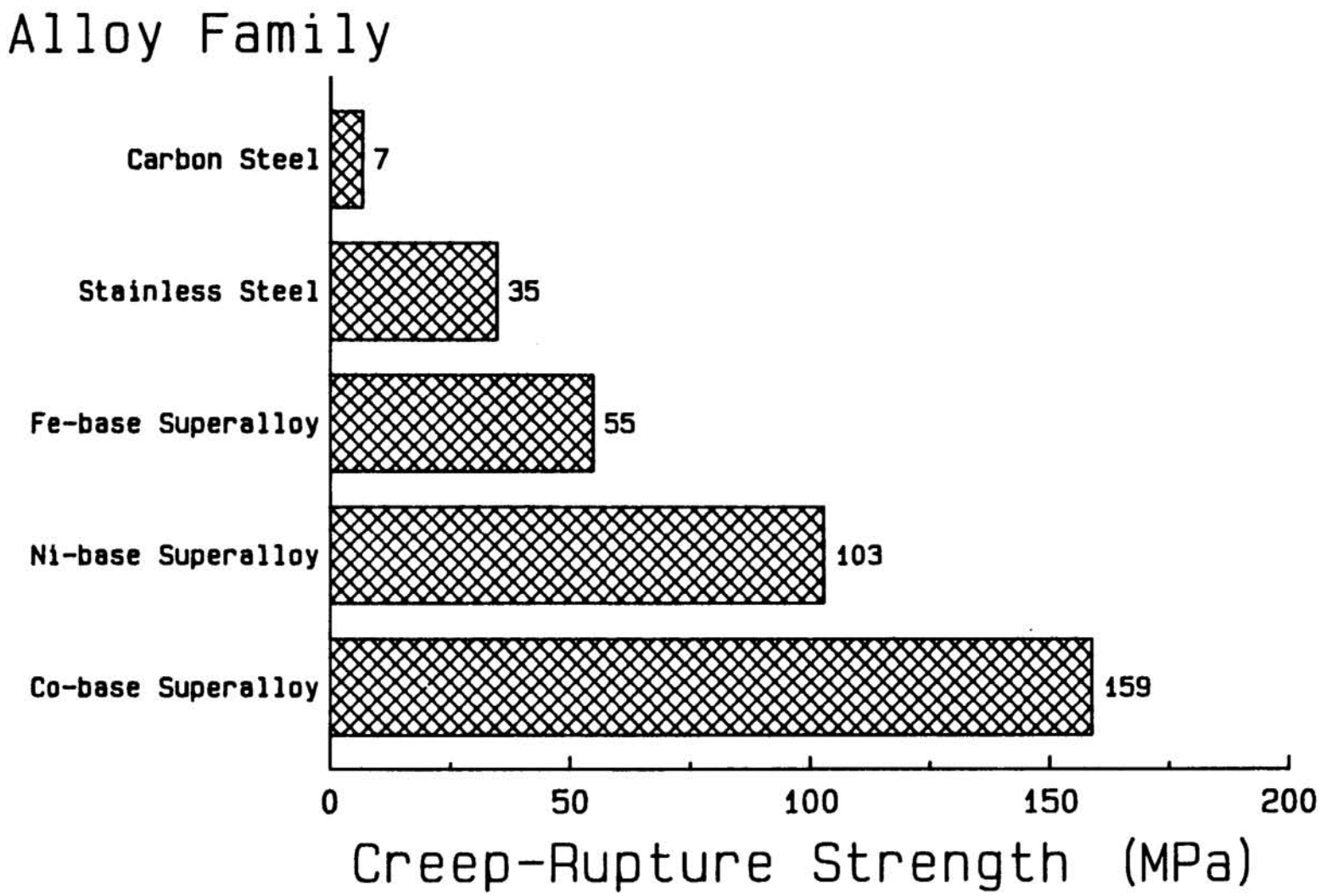

Figure 2. Creep-rupture strengths (MPa) of alloy families after 100 hours at 850°C (ASM Metals Handbook, 1978).

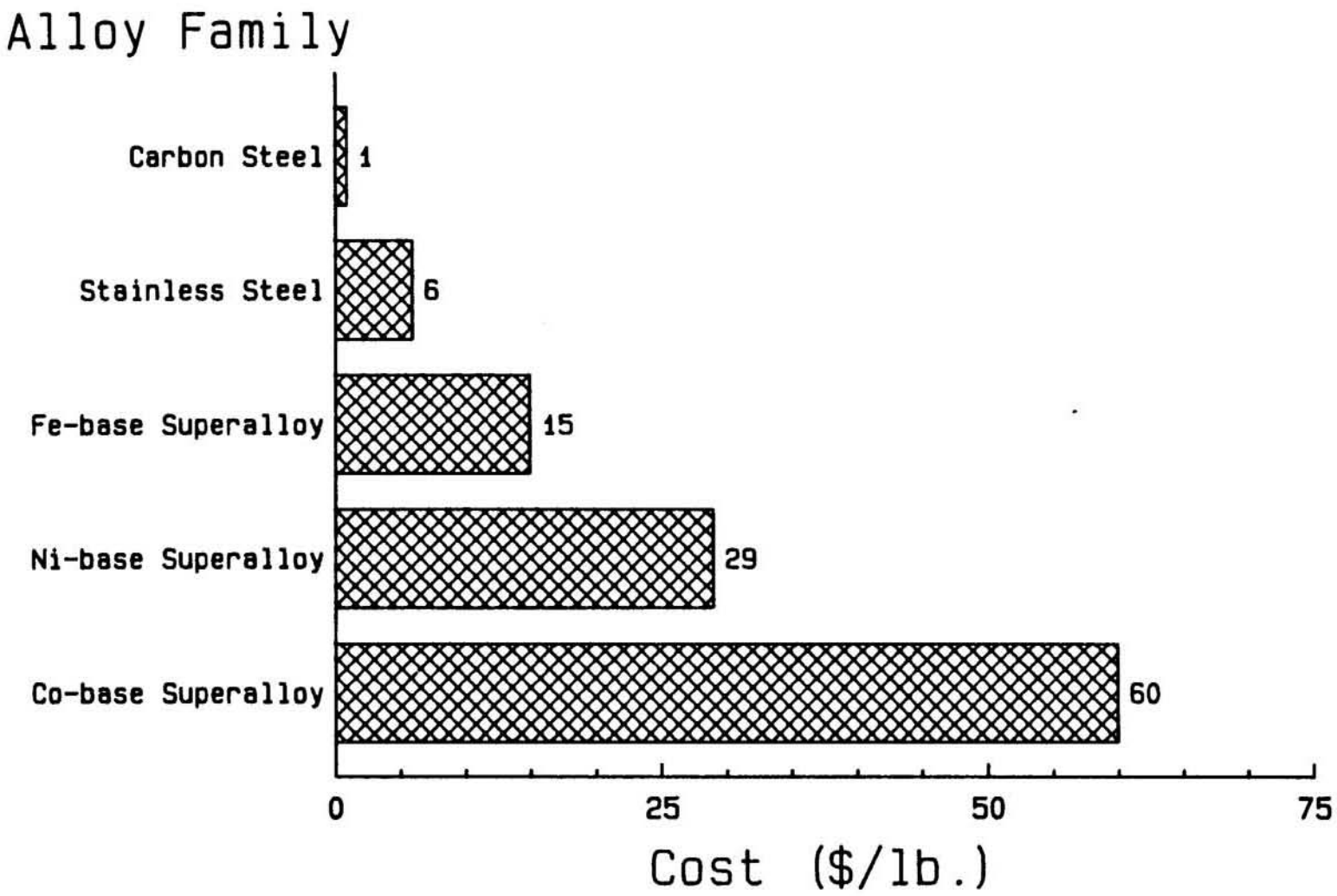

Figure 3. Alloy family cost ($/lb) for 20 mm OD (8 inch), schedule 160 pipe (industry quote, 1985).

rupture-life and chemical resistance at high temperature, they would be prohibitively expensive in large quantities for magma energy applications. The intent is therefore to find an alloy with satisfactory mechanical and chemical properties for the least cost.

The next three alloys in Table 3 are very different from the majority of the other Fe-Ni-Co high temperature alloys investigated. Kanthal A-1, Nimonic 105 and Cabot 214 all contain sufficient aluminum (above 5 wt %) to be alumina formers in an oxidizing environment. They also contain sufficient chromium (near 15 wt %) to be chromia formers as well. The combination of the two external scales (both alumina and chromia) usually increases the oxidation resistance of an alloy significantly. These alloys are also characterized by very good strength at high temperature.

The remaining five materials listed in Table 3 are alloys based on a refractory metal such as molybdenum, tantalum or zirconium, or other nearby periodic table metals such as titanium and rhenium. TiCode 12 is a popular titanium alloy which has excellent chemical resistance to salt brines at moderate temperatures. T-111 and Zircaloy-2 are alloys based on the refractory metals tantalum and zirconium, respectively, which have good moderate temperature strength and oxidation resistance. The refractory metals molybdenum and rhenium were tested because of their excellent corrosion resistance in basaltic magmas (see Douglass, 1983) and their potential use as thermocouple wire.

3. Environment-material experimental matrix

The 17 materials, together with the magmatic and subsolidus environments, define an experimental test matrix that is large, expensive, and time consuming to complete. Ability to survive in magma in the event of loss of coolant, however, provides a criteria for restricting the number of candidate alloys and tests. Therefore, the initial compatibility tests were performed in magma under both fluid saturated and undersaturated conditions at 850°C and 200 MPa for a run duration of 7 days. Examination of these tests provided information about metal corrosion processes. Although unacceptable rates of general corrosion have not been defined, some forms of localized corrosion (e.g., intergranular) are undesirable. Likewise, exact design criteria for mechanical strengths have not been specified, although it is thought that minimal creep rupture strengths need to be in excess of about 40 MPa. Cost estimates for a 300 m long heat exchanger have not been made. However, combining the results from compatibility tests with mechanical strength and cost estimates provide the basis for eventually limiting compatibility tests to 3-6 alloys.

4. Sample preparation

A rhyolite starting material containing reconstituted magmatic volatiles comparable to those expected in rhyolite at depth for Long Valley and Coso was obtained by melting powdered Panum Crater obsidian (Table 1) at high pressure in the presence of a solution bearing H_2O, F, Cl, S, and CO_2. Dense, bubble-free

rhyolite glasses with reconstituted magmatic volatiles representing saturated and undersaturated conditions were synthesized in sealed noble metal bags at 850° and 325 MPa for 3 days using a large volume internally heated pressure vessel. The volatile concentrations of these experimental glasses and of natural samples from Long Valley and Coso are given in Table 2.

In the magma-metal compatibility tests, finely powdered rhyolite (particle size <10 μm) containing the reconstituted volatiles is placed in a gold bag (3.8 mm OD x 20 mm long) along with a short section of the test alloy wire (0.8-2.0 mm OD). Ten percent, by weight, deionized water is added to ensure fluid saturated conditions, and the capsule is welded shut in order to chemically isolate the system (Fig 4). A similar sample preparation is used in rubble-metal tests, but the size of the rhyolite rubble is increased to 75-500 μm. In the glass-metal tests, polished glass plates containing reconstituted magmatic volatiles are bound on either side of a doubly polished section of the test alloy with thin platinum wire. The entire assembly is sealed inside a gold metal bag (Fig. 5) by DC arc welding using a moist tissue to cool the gold tubing during welding and prevent volatile loss. Charges that show significant mass changes before and after welding and vacuum oven drying are assumed to have leaked volatiles and are discarded. In addition, capsule integrity is checked before and after a run by visual examination

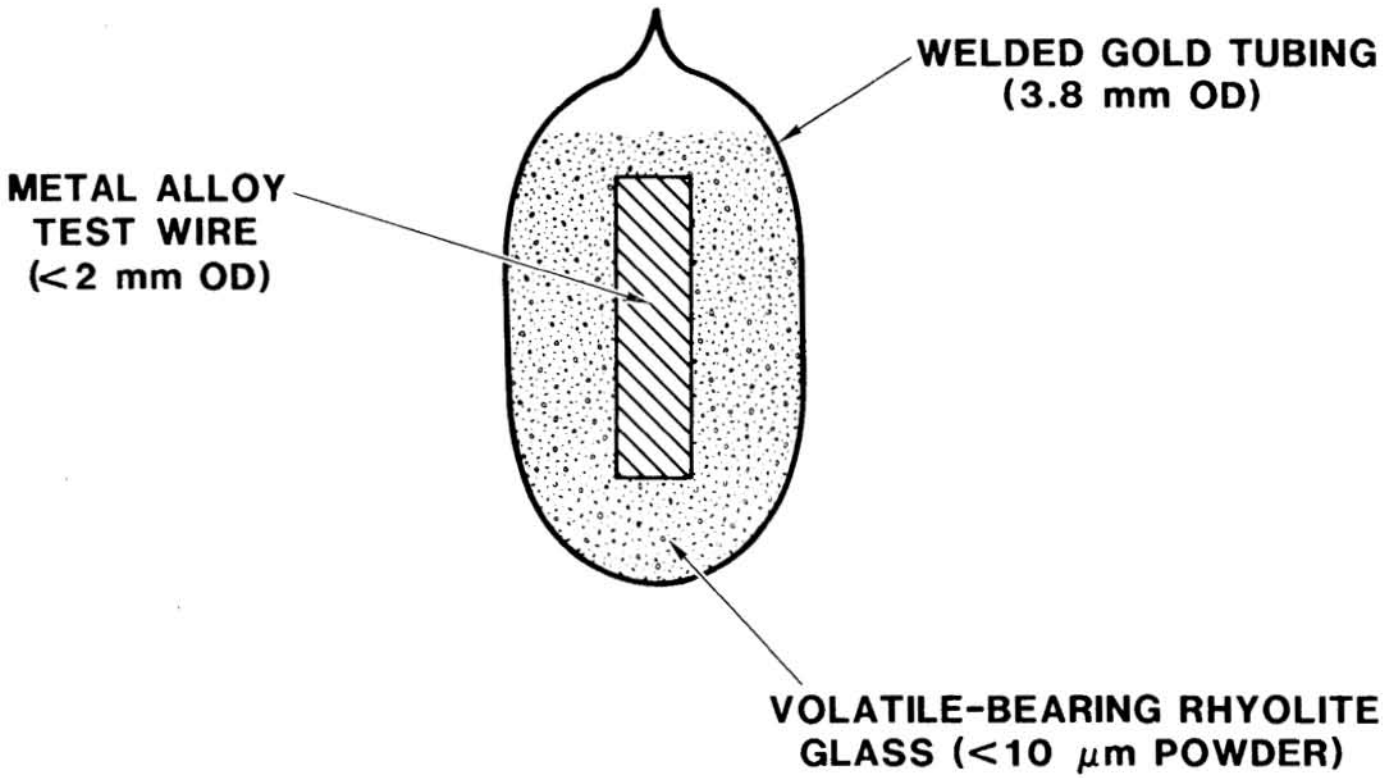

Figure 4. Schematic of sample configuration for magma-metal compatibility tests.

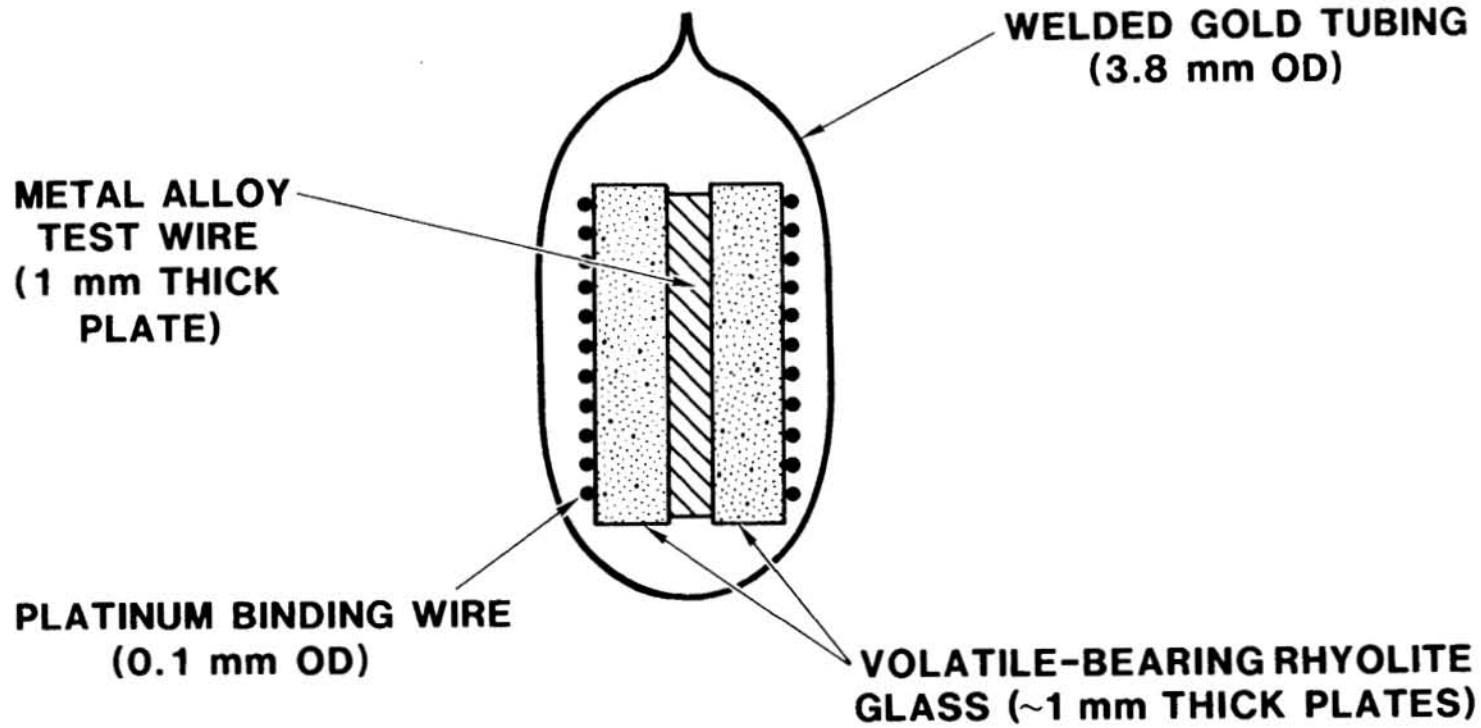

Figure 5. Schematic of sample configuration for glass-metal compatibility tests.

using a binocular microscope and by comparisons of pre- and post-test masses.

5. Experimental facilities

The reconstitution of volatiles to rhyolite glass from Panum Crater as well as most magma-metal compatibility runs are performed using internally heated pressure vessels (Fig. 6). These vessels have an internal platinum or molybdenum furnace surrounded by a water-cooled pressure vessel. This configuration allows for a generous internal sample cavity which permits use of a large sample capsule or several small samples that are run simultaneously. A unique extra-large volume (~700 ml) facility at Sandia Labs. is utilized for batch magma-metal runs of the entire metal test matrix and for synthesizing large quantities (10-20 g) of the volatile reconstituted rhyolite glass.

Most glass-metal and rubble-fluid-metal tests are conducted in cold seal pressure vessels (Fig. 7). These pressure vessels employ an external furnace for heating and are convenient for runs of long duration because of their simple and durable metal cone seals. In addition, cold seal pressure vessels are adaptable to specialized applications, such as the flowing rubble-fluid-metal experimental configuration for examining mass transport effects in direct contact heat exchangers (Fig. 8). In these tests, a long pressure vessel is used to simulate the P-T environment in the fractured glassy rubble surrounding a direct contact heat exchanger. Heat flow characteristics of the system,

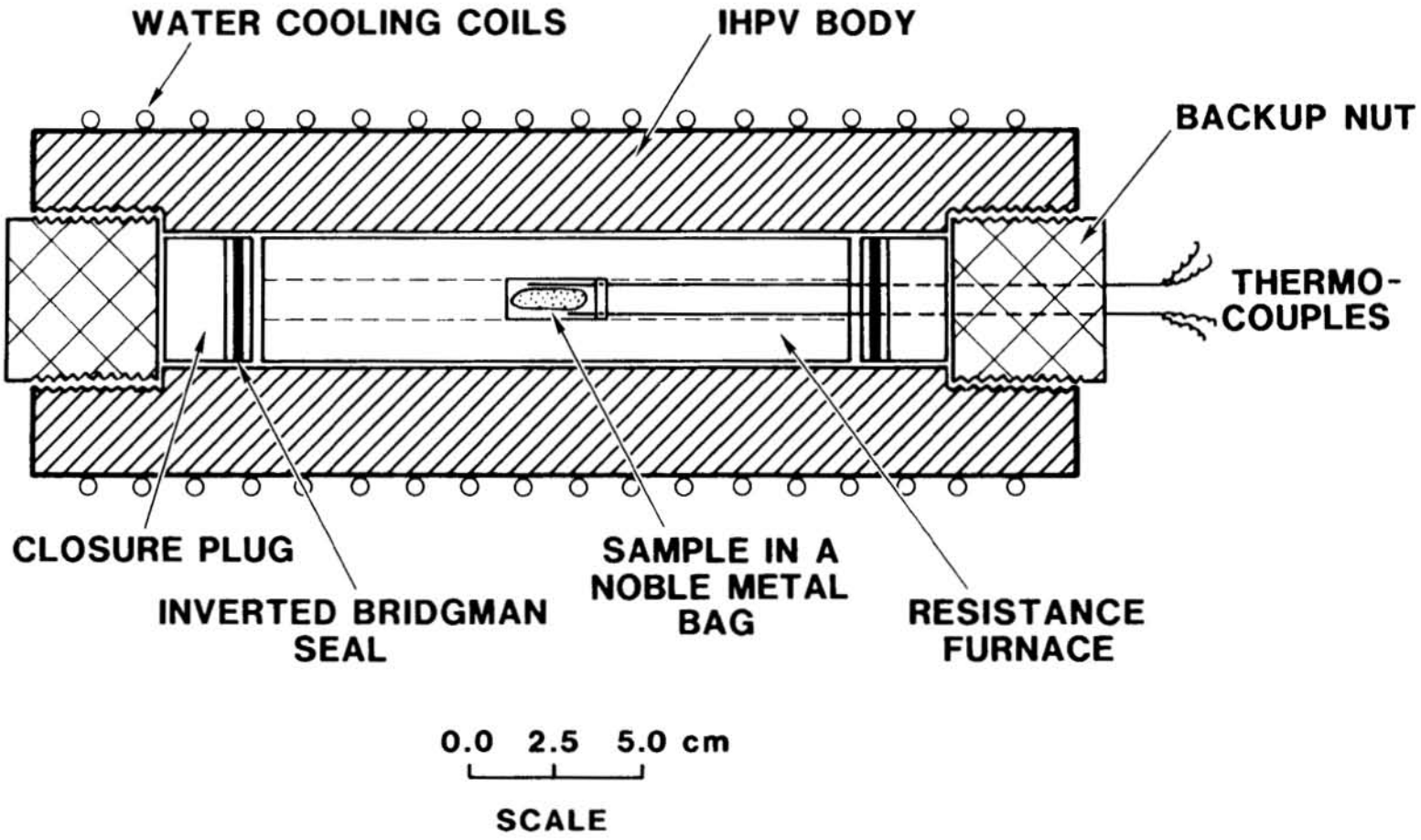

Figure 6. Schematic of an internally heated pressure vessel (IHPV) used in magma-metal compatibility tests.

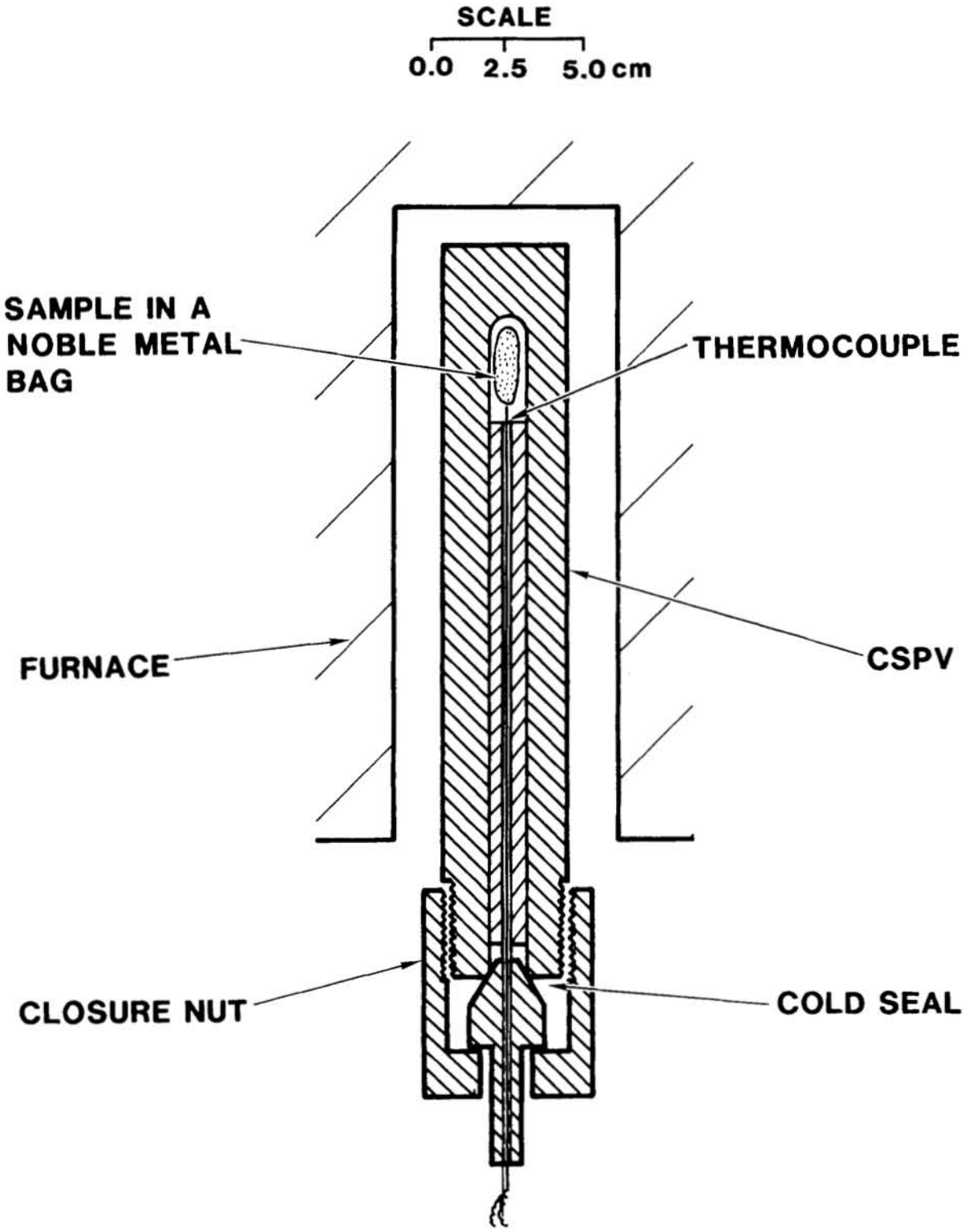

Figure 7. Schematic of cold seal pressure vessel (CSPV) used in glass-metal and rubble-fluid-metal compatibility tests.

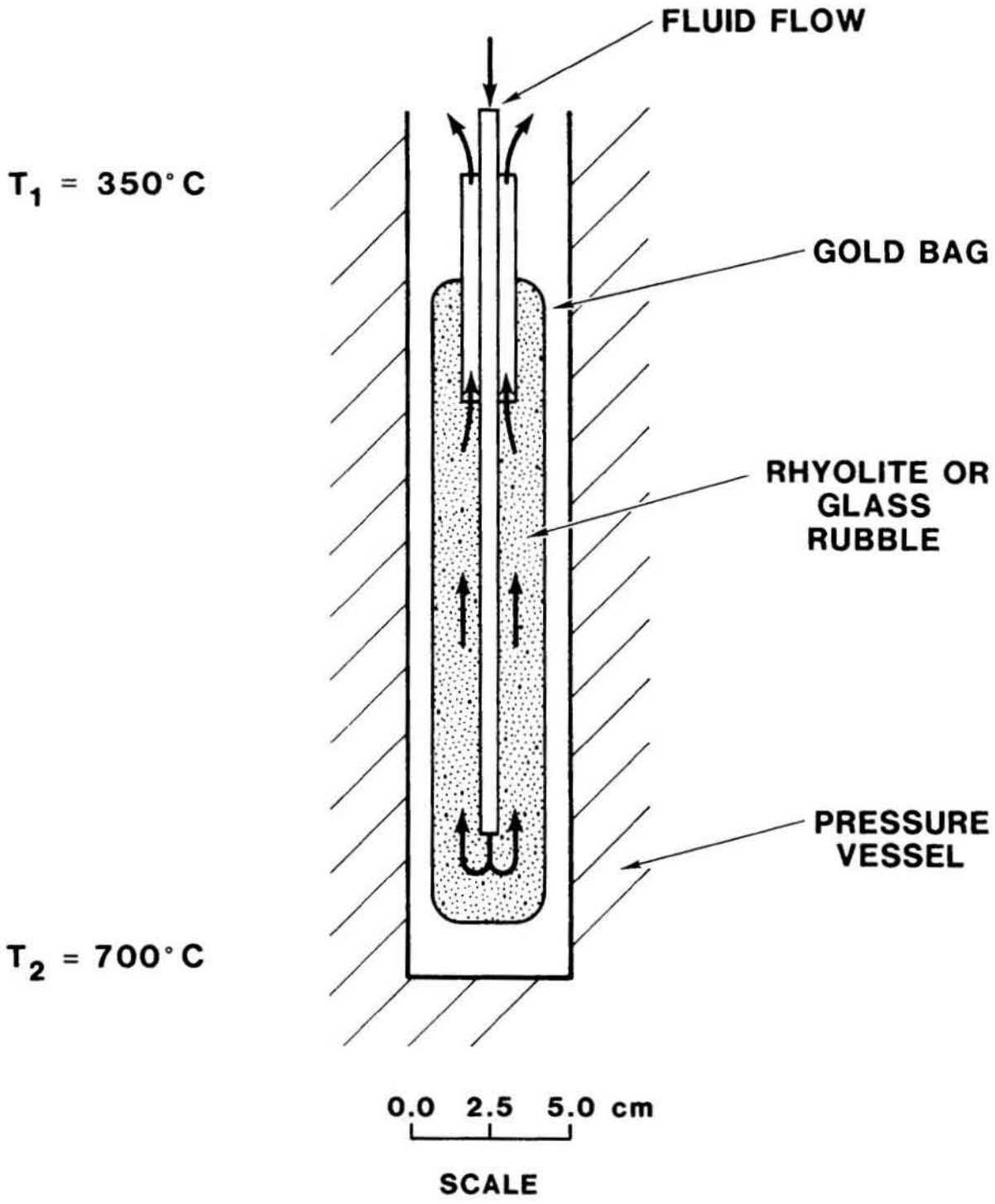

Figure 8. Schematic of cold seal pressure vessel configuration for investigating chemical transport effects in direct contact heat exchangers.

radially through the rubble or vertically along fluid flow paths, can be scaled to laboratory dimensions to characterize and evaluate potential dissolution/precipitation and transport problems.

6. Data acquisition

After reaction in a pressure vessel, sample capsules are examined and weighed to detect leaks and then cut open. If the sample appears friable, it is left in the capsule and impregnated with epoxy; all samples are then removed and cast in epoxy mount. After cross sectioning, the sample surfaces are polished to 1 μm in preparation for optical and electron microscopy. Reflected light photomicrographs are taken with a Leitz metallograph microscope at 50, 100, or 500x magnification; transmitted light examinations of any polished thin sections are made using a Leitz polarizing microscope. Most analytical work is performed using a fully-automated Cameca MBX electron microprobe equipped with secondary electron (SE) and backscattered electron (BSE) detectors, an energy dispersive spectrometer (EDS), and three wavelength dispersive spectrometers (WDS). Imaging capabilities include SE, BSE, and identical area elemental micrographs (commonly called elemental distribution photomicrographs or EDPM's), and quantitative spot analyses. SE photomicrographs taken at 100 to 800x magnification illustrate surface features while BSE photomicrographs emphasize density contrasts; EDPM's clarify BSE photos by providing element specific scans. EDPM's coupled with SE and BSE photos are used to locate and identify

reaction rinds and metal grain boundary decorations, while spot analyses are used for chemical characteration.

7. Preliminary tests

Preliminary tests were begun in FY1984 on 1095 high carbon and 310 stainless steels to obtain estimates of experimental run durations required for sufficient development of reaction products. These experiments also tested sample preparation procedures, experimental techniques, and analytical methods.

FY1985 Activities

1. Results of tests in magma

In FY 1985, 29 "preliminary" magma-metal tests were completed on 1095 steel and 310 stainless steel for run durations ranging from 30 minutes to 28 days at 850°C and 100 MPa. Most of these runs were at fluid-saturated conditions. Batch runs using the 17 test metals were made at fluid-saturated and fluid-undersaturated conditions at 850°C and 200 MPa for durations of 7 days. Runs of longer duration and at higher than expected volatile concentrations are planned for FY86 to examine long term corrosion rates and reactions.

Figure 9 shows the results from electron microprobe analyses of the 1095 carbon steel tested in magma, saturated with volatiles, at 850°C and 200 MPa for 7 days. The backscattered

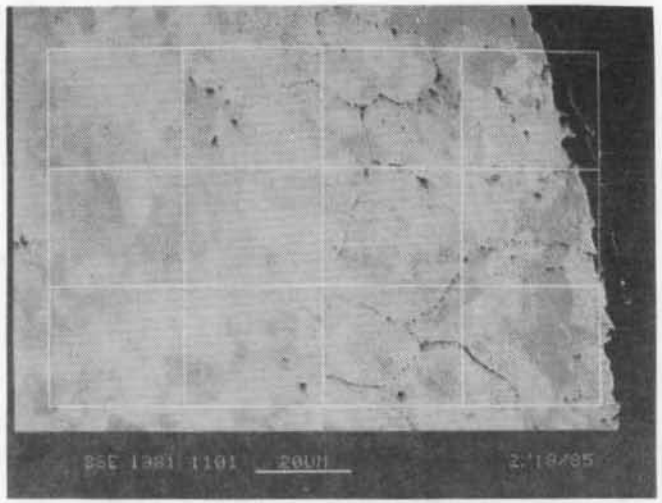

BSE PHOTOMICROGRAPH

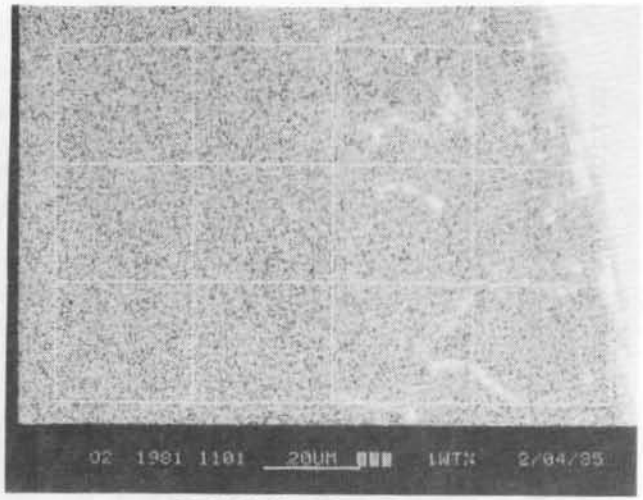

OXYGEN EDPM

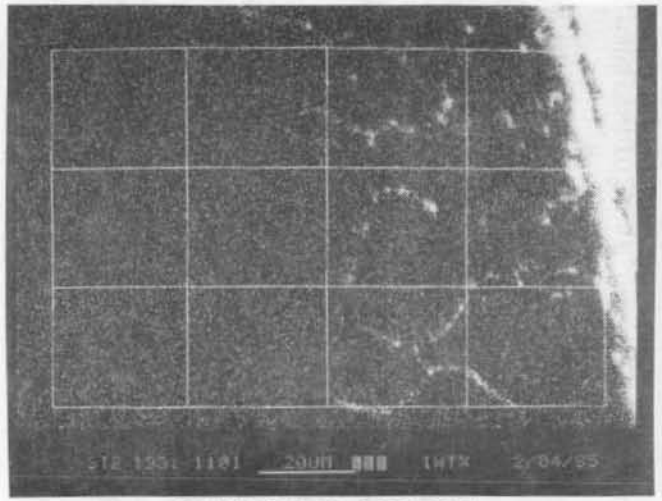

SILICON EDPM

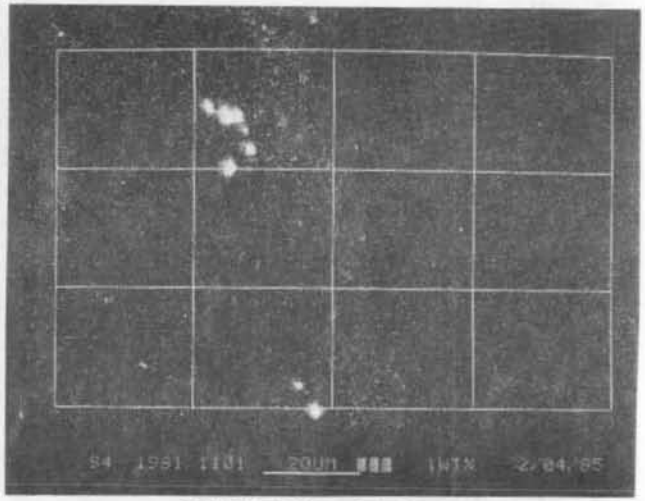

SULFUR EDPM

Figure 9. Electron microprobe analyses of 1095 carbon steel tested in volatile-saturated magma at 850°C and 200 MPa for 14 days. The BSE photomicrograph depicts severe decoration of grain boundaries; element maps for oxygen (02) and silicon (SI2) shows that the grain boundary phase contains oxygen and silicon; sulfur (S4) element map depicts extensive sulfur remobilization (all at 800X).

electron micrograph of the steel wire shows a severe decoration of the grain boundaries (up to 80 μm penetration from the exterior). The accompanying electron distribution photomicrographs (EDPM`S) identify a grain boundary species containing silicon and oxygen, either as silica or silicate (obvious magmatic components). The EDPM for sulfur indicates that the sulfur in the steel (originally ca. 170 ppm) is being remobilized by the advancing oxygen zone and is not contributed by the rhyolite magma. This observation was corroborated by additional water-1095 steel tests, where there is evidence of extensive sulfur remobilization ahead of the steel's oxidized exterior. Sulfidation, therefore, does not appear to be an inherent corrosion problem in rhyolite melts, in contrast to material tests in basalts (Douglass and Healey, 1979; Douglas and Ehrlich, 1982; Douglass, 1983).

Figure 10 shows the results from electron microprobe analyses of the Inconel 625 tested for 7 days in magma saturated with volatiles, at 850°C and 200 MPa. These results are broadly representative of those observed for most of the iron-base, nickel-base and cobalt-base superalloys as well as 310 SS. The backscattered electron photomicrograph at the magma-metal interface shows very little decoration of the grain boundaries (10-15 μm wire penetration). This is confirmed by the absence of an enhanced oxygen X-ray signal at the grain boundaries in the oxygen EDPM. There are enhanced oxygen and chromium X-ray signals at the magma-metal interface, (see Figure 10), indicating

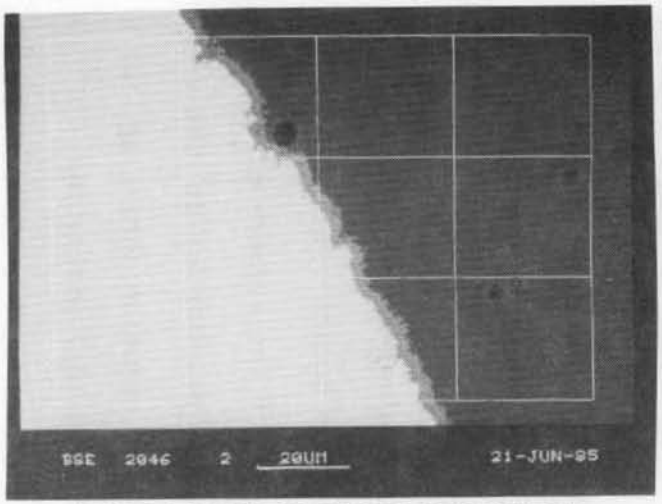

BSE PHOTOMICROGRAPH

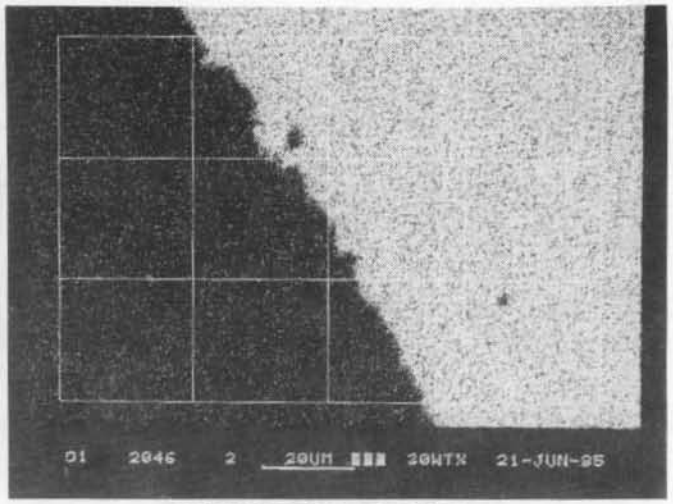

OXYGEN EDPM

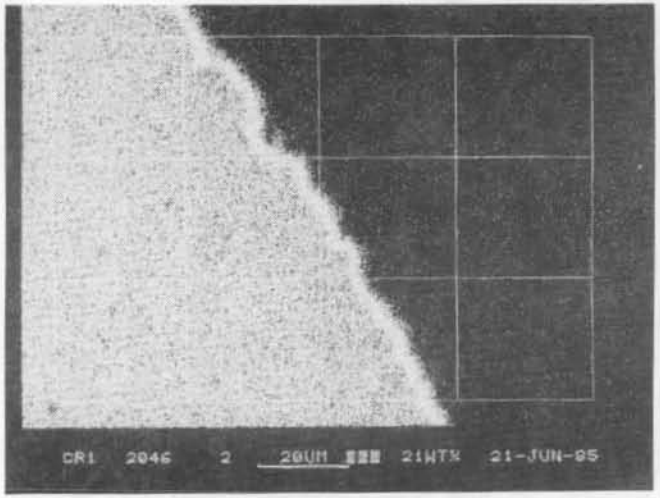

CHROMIUM EDPM

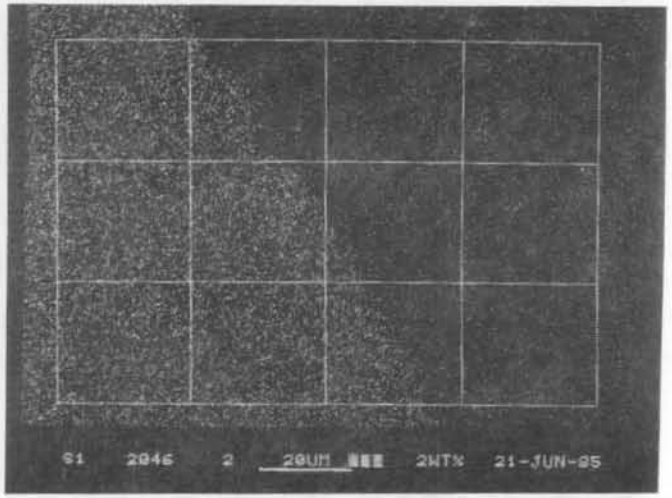

SULFUR EDPM

Figure 10. Electron microprobe analyses of Inconel 625 tested in volatile-saturated magma at 850°C and 200 MPa for 7 days; BSE maps and EDPM's depict simple oxidation with little grain boundary penetration (all at 800X).

the presence of a chromia film. The EDPM for sulfur shows no sulfidation either by sulfur penetration from the magma or by sulfur remobilization within the material. The lack of sulfur remobilization, compared to 1095 carbon steel, probably reflects the relatively low concentrations of sulfur in these alloys (< 35 ppm) and the limited depth of metal oxidation. The 310 stainless steel gave results similar to the iron-base alloy RA 330 which shows a small amount of grain boundary penetration by oxygen. The 304 and 26-1 stainless steels exhibit significantly more penetration of the grain boundaries by oxygen/silicon. All of these stainless steel alloys formed a chromia film at the metal/magma interface.

Results from tests done on alloys which are both alumina and chromia formers, such as Nimonic 105, Kanthal A-1 and Cabot 214, indicate that very little, if any, grain boundary penetration by oxygen has taken place. The external oxide scale consisted of distinct alumina and chromia layers, the aluminum oxide being adjacent tothe metal and the chromium oxide bordering the silicate melt. An iron-rich rind outside of the alumina-chromia external scale is relatively thin compared to that formed on the more reactive alloys.

All refractory metals and alloys were severely oxidized in just seven days in the volatile-saturated magma environment. The TiCode 12 wire (1 mm OD) was almost completely consumed during the test. The T-111, molybdenum and zircaloy-2 oxidized about equally with approximately 50 μm of metal consumed in the seven

days. Rhenium exhibited the most corrosion resistance of this group, but it showed evidence of severe metal recrystallization, thereby allowing oxidation of the metal to depths up to 200 μm. Therefore, none of these materials appears to be usable in a rhyolite magma environment.

Tests for the above materials in volatile-undersaturated but otherwise similar environmental conditions gave similar results for metal corrosion as those obtained in volatile-saturated magma. However, reaction progress was usually less developed for an equivalent exposure time within any family of alloys, probably because reactions are limited by oxygen and metal ion diffusion through solid phases (silicate or oxide).

The volatile-bearing rhyolite melt reacted readily with all test alloys. From runs using 1095 steel, reaction rind growth mechanisms were identified. A mixed silicate-oxide reaction rind consisting principally of large (generally tabular) fayalite crystals (Fe_2SiO_4) in an open structure with interstitial hercynite ($FeAl_2O_4$) form initially on the 1095 steel as a result of a surface controlled silicate melt-metal reaction (Fig. 11). The silicon, aluminum, and oxygen are supplied by the magma and the iron is contributed by the 1095 steel. With time, this surface-controlled process is replaced by a volume diffusion process with the formation of magnetite at the edge of the euhedral fayalite crystals (Fig. 11). Figure 12 is a time sequence of photomicrographs providing a reflected light view of the progress of the reaction growth from 1 to 14 days. A "zero time" run (not

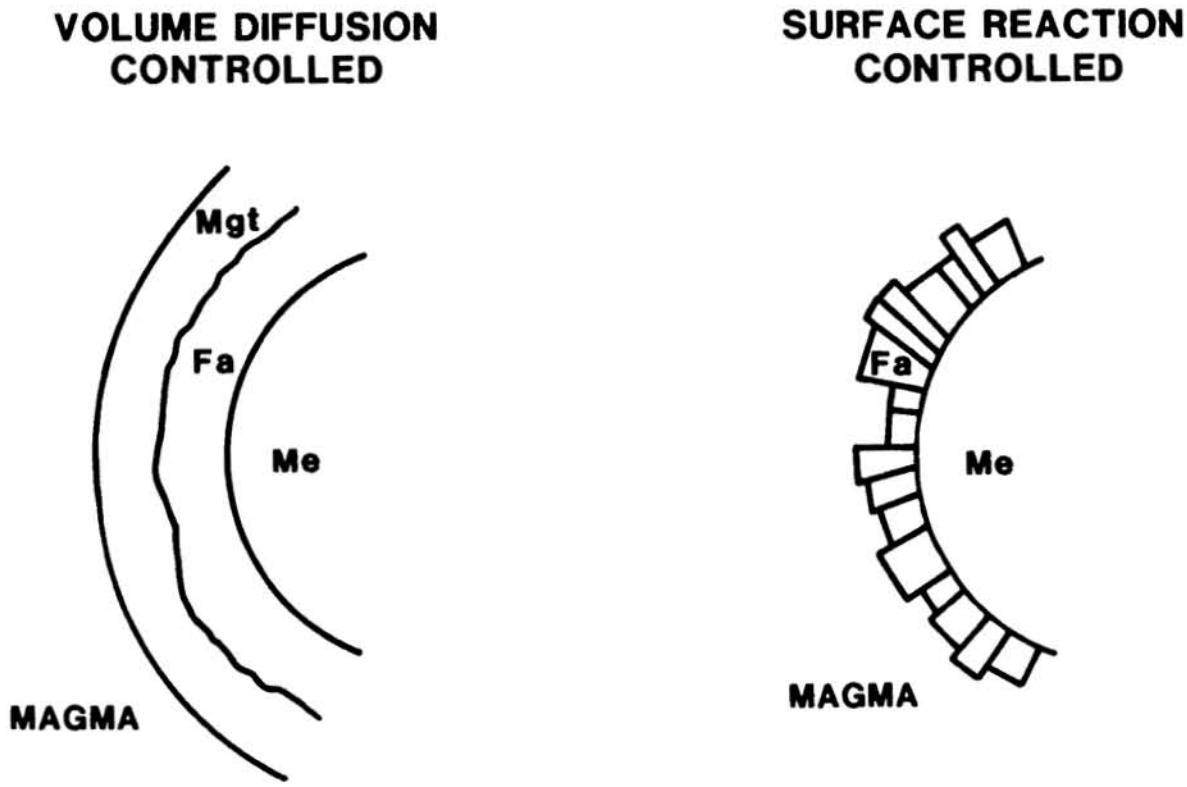

Figure 11. Rind growth mechanisms for reaction between magma and metal (Me) to form fayalite (Fa) and magnetite (Mgt).

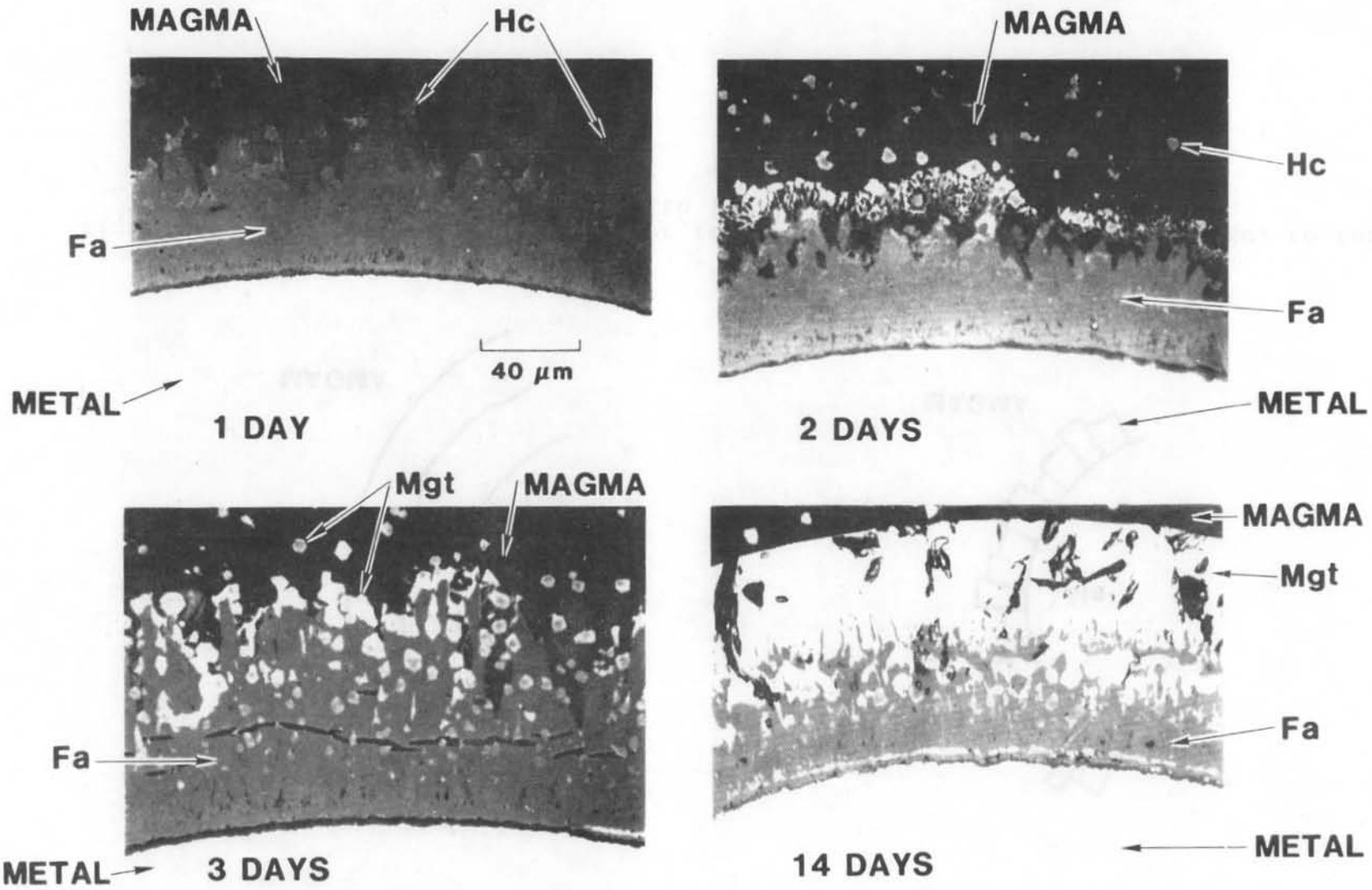

Figure 12. Progress of reaction rind growth for 1095 steel in volatile-saturated magma at 850°C and 100 MPa. Phase compositions are described in the text for fayalite (Fa), magnetite (MGT), and hercynite (Hc).

shown) exhibited a 5 μm thick fayalite-spinel rind. After 1 day of exposure to the magma, hercynite also appears in the melt as isolated crystals and starts to form a continuous rind at the edge of the advancing fayalite growth. After 2 days of reaction, hercynite at both locations is altered to magnetite (Fe_3O_4) by the exchange of Al^{3+} for Fe^{3+}. After 3 days, the fayalite growth is 80 to 100 μm thick with the melt-metal interface being completely dominated by the magnetite. Hercynite still is present but now as an interior phase in the fayalite rind. With 14 days of reaction, the magnetite phase dominates the reaction rind (now over 100 μm thick) with the complete conversion of hercynite to magnetite and the growth of magnetite from the fayalite. Long term magnetite rind growth rates were observed to be as high as 15 μm/day, while oxide/silicate penetration in 1095 steel was found to be about 0.5 μm/day.

Textural evidence suggests that the 1095 steel developed an initial fayalite rind by a surface-controlled process, which after 3 to 6 days, is replaced by a volume diffusion process. This is demonstrated by the smooth and continuous nature of the magnetite-magma interface and by the large grain structure of the magnetite as highlighted by the interference contrast reflected light photomicrograph of a 14 day test (Fig. 13). Electron microprobe analyses of the glass (melt) near the magma-metal interface have determined the existence of a gradient in iron from this interface into the bulk of the glass. A complementary oxygen gradient is inferred from the iron data. These data

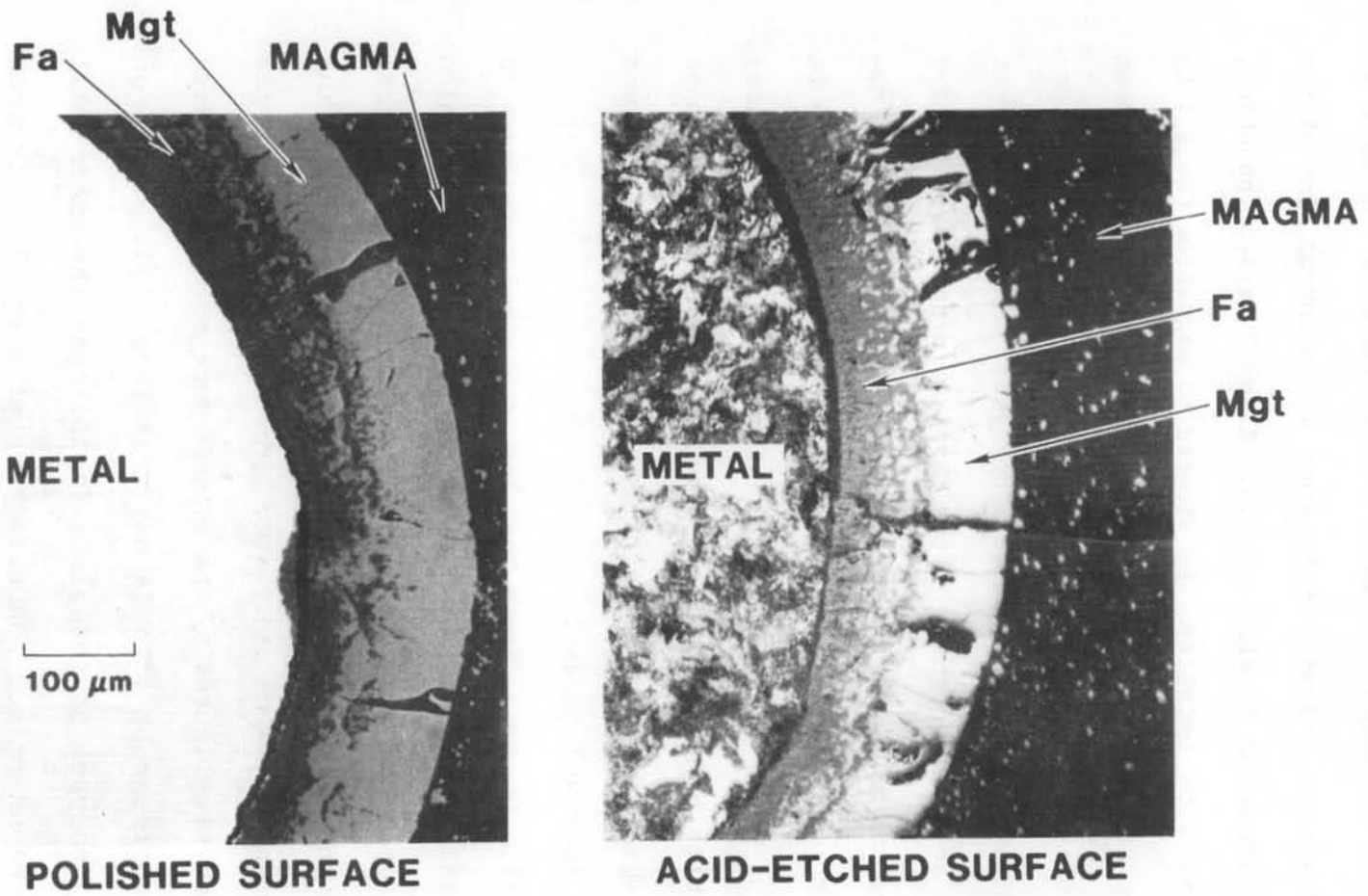

Figure 13. Reflected light (left) and interference contrast reflected light (right) photomicrographs (200X) showing smooth and continuous magnetite-magma interface and large grain size of magnetite for 1095 steel subjected to magmatic conditions at 850°C and 100 MPa for 14 days; Fa and Mgt refer to fayalite and magnetite, respectively.

indicate the flux of iron outward from the metal, through the fayalite and magnetite layers accompanied by the appropriate oxidation state changes, and into the magma (Fig. 14). Conversely, oxygen is transported from its source region, the magma, to the metal. Large changes in oxygen fugacity would occur at the spinel/fayalite and at the fayalite/metal phase boundaries. Thus, the rate-limiting step for rind growth is mutual and opposite volume diffusion of Fe and O through the reaction rind between the silicate melt and the 1095 steel. Figure 14 provides a schematic of the rind phases that form on the steel surface; the diffusion controlled reactions and corresponding mass fluxes are indicated along with the valence states of iron in each of the phases.

In contrast to the high reactivity of the 1095 steel with components of the silicate melt, as shown by the fayalite-hercynite rind, other alloys, like 310 stainless steel, exhibit simple oxidation-reduction reactions. A solid solution of chromium, manganese and iron oxide forms adjacent to the metal providing an effective barrier to minimize continued reaction between the magma and the metal. A sparse layer of iron oxide was detected in the melt immediately adjacent to the metal oxide scale. Rind growth appears to be by volume diffusion of Fe, Mn, and Cr outward into the melt and inward diffusion of oxygen. Growth rates and metal penetration rates are significantly reduced (by an order of magnitude) compared to those observed for

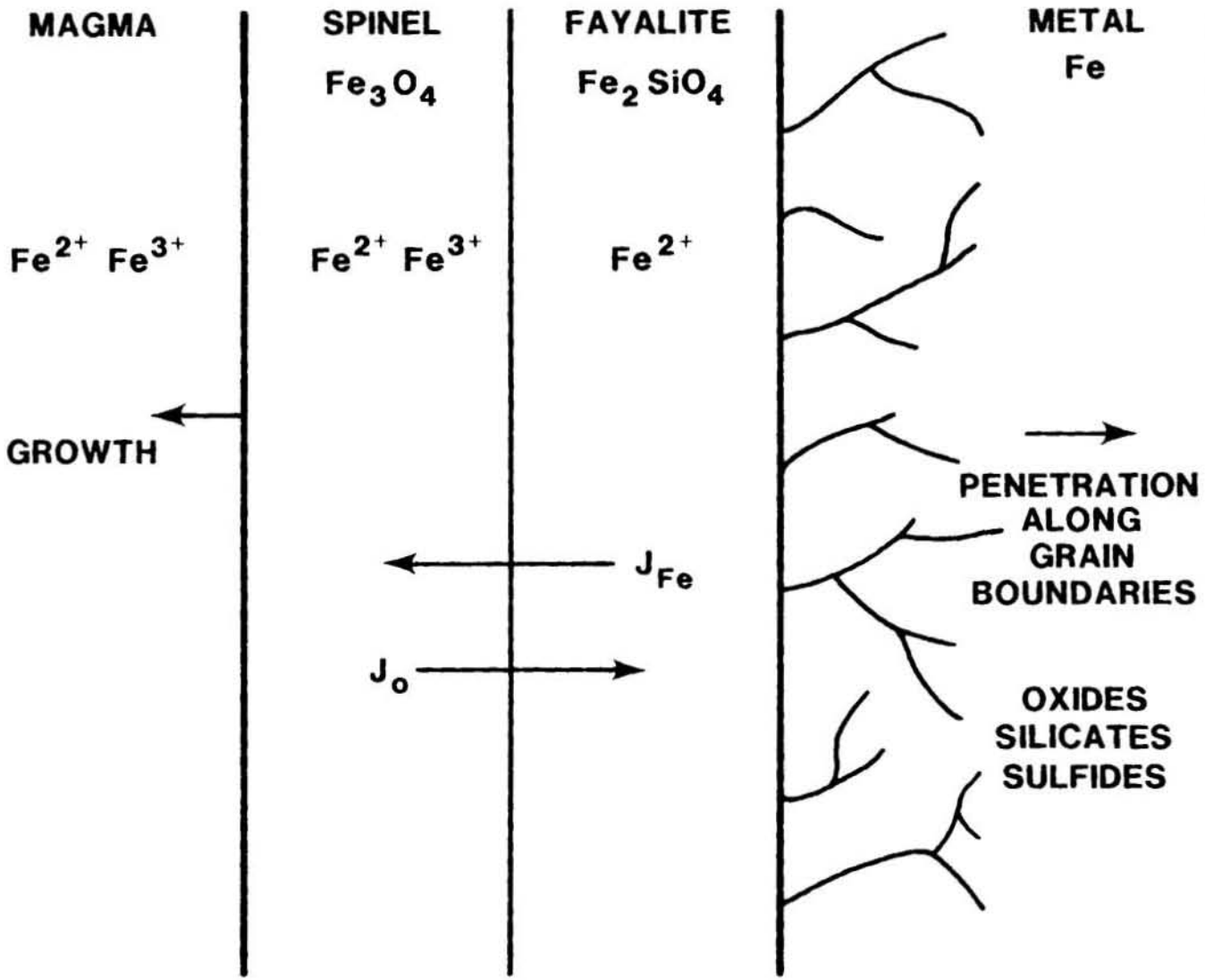

Figure 14. Schematic of diffusion controlled processes responsible for formation of reaction rind phases. J_O and J_{Fe} show fluxes of oxygen and iron, respectively.

1095 steel. Figure 15 compares the reaction rinds for 1095 steel and 310 stainless steel after 14 days at 850°C.

The experiments with undersaturated rhyolite magma and 1095 steel exhibit moderate fayalitic rind formation; however, a spinel (hercynite-magnetite) rind did not form (Fig 16). Numerous vapor bubbles were noted in the magma for unsaturated conditons (Fig. 17). Numerous small bubbles are homogeneously distributed throughout the melt and are thought to be an artifact of air entrapment in the powdered starting material during melting. This feature was not evident in the vapor-saturated glasses probably because of the lower surface tension at the melt vapor (water rich) interface. Bubble nucleation and growth at the magma-metal interface was also observed in many of the fluid-undersaturated runs. After several days, the bubbles would grow, coalesce and gradually migrate away from the magma-metal interface. Some capsules eventually burst due to the generation of high internal vapor pressures. Mass spectroscopic analysis of the vapor liberated from crushed samples of the glass identified the bubble vapor composition to be predominantly carbon dioxide. Since there is very little carbon present in the rhyolite (<5 ppm), oxidation of carbides in the steel is the most probable source for the CO_2-rich bubbles.

2. Results of tests in volatile-bearing glass

Seven preliminary glass-metal tests were completed at 500°C and 50 MPa using 1095 steel and 310 stainless steel. These tests

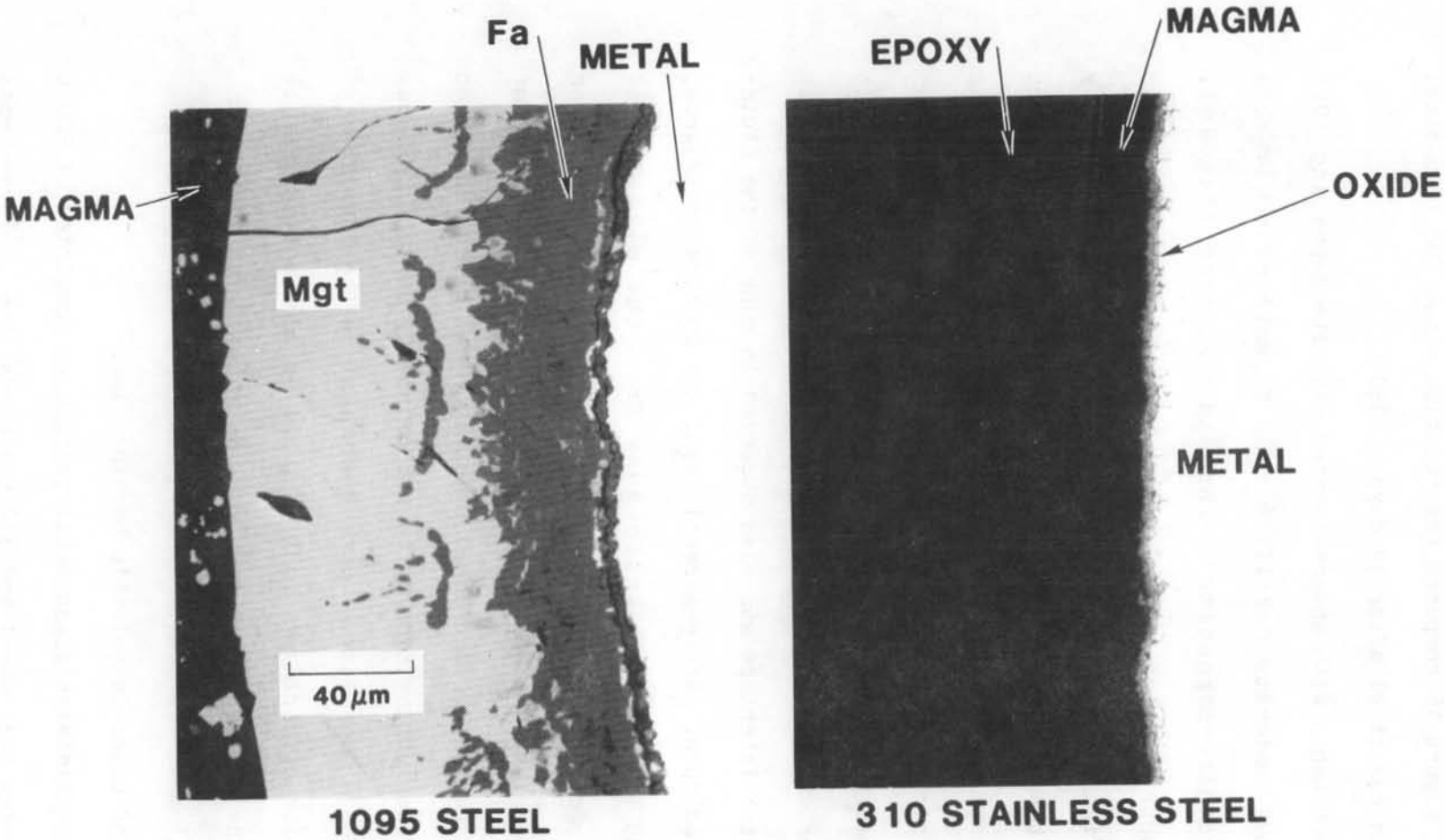

Figure 15. Comparison of reaction rind growth rates for 1095 steel and 310 stainless steel in magma at 850°C and 100 MPa for 14 days (500X photos). The phases present are magma, metal, oxide, fayalite (Fa), magnetite (Mgt) and epoxy.

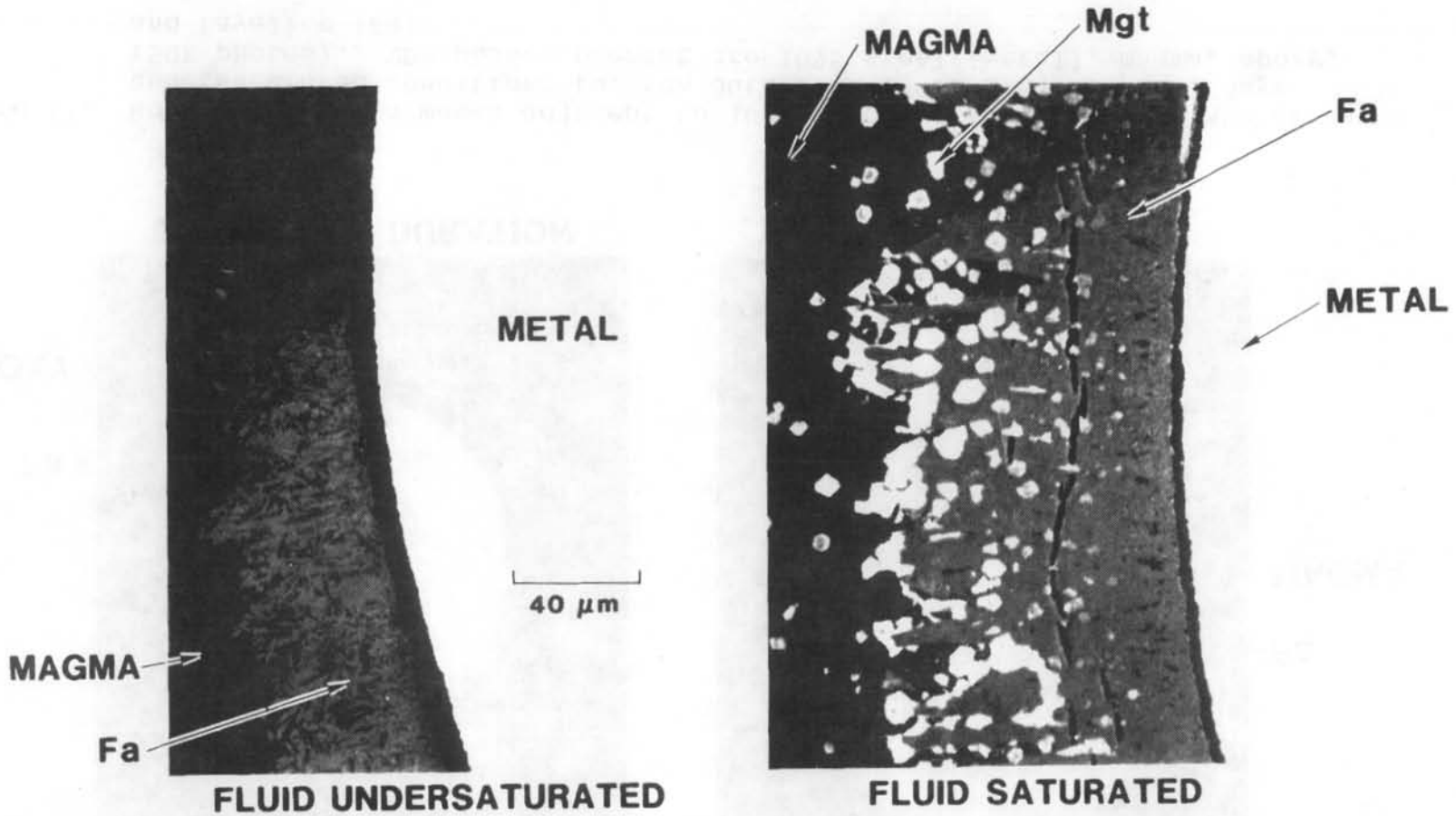

Figure 16. Comparison of reaction rind development for 1095 steel in magma (850°C, 100 MPa, 3 days) for undersaturated and saturated conditions (500X photos). The phases present are 1095 steel (metal), magma, fayalite (Fa), Magnetite (Mgt).

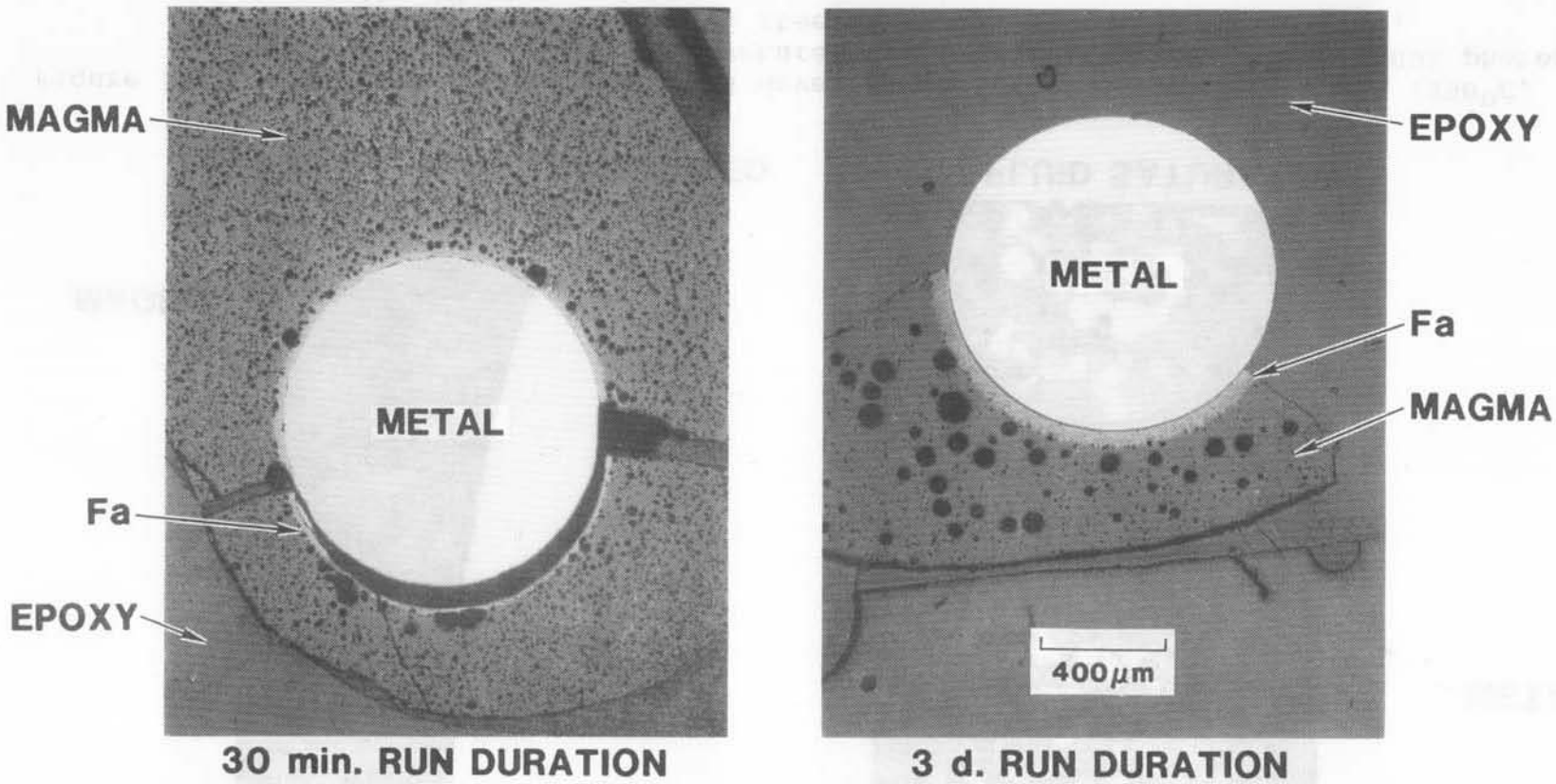

Figure 17. Bubble growth in magma adjacent to 1095 steel at 850°C and 100 MPa at vapor-undersaturated conditions for run durations of 30 minutes and 3 days (50X photos). The phases present are 1095 steel (metal), magma, epoxy, and fayalite (Fa).

were for durations of 1 to 28 days with the glass-metal-glass "sandwich" sample configuration (Fig. 5). In glasses containing 3.0 wt.% volatiles, vapor bubbles were formed after one day at 500°C in response to the high internal water vapor pressure of the glass; 9 to 14 days were required for initial bubble nucleation in glasses with 1.5 wt.% volatiles (Fig. 18). A vapor phase (not identified) formed at the glass-1095 steel interface, probably as a result of a redox reaction, and grew with time. This feature is not well developed at the interface of the glass-310 SS run. Vapor bubbles in the glass and at the glass-metal interface are significantly larger in those glasses containing more dissolved volatiles. In addition, voids were noted in the interior of 1095 steel after a long run of 28 days. EDPM analyses of this sample has shown that these rinds are not the result of **in situ** metal oxidation. Void development at this interface may be related to a redox reaction between hydrous glass and metal, resulting in liberation of hydrogen and its subsequent adsorption in the steel. Plastic deformation of the hydrous glass is also apparent from the change of the once-flat glass surface about the platinum binding wire (Fig. 18) and might prove to be a critical factor for migration of hydrothermal fluids in a direct contact heat exchanger. Resistence to corrosion was excellent in all tests. Only a very thin reaction rind (< 5 μm thick iron oxide) was noted at the glass-steel interface, even after 28 days; no grain boundary penetration of the 1095 steel was found. This is

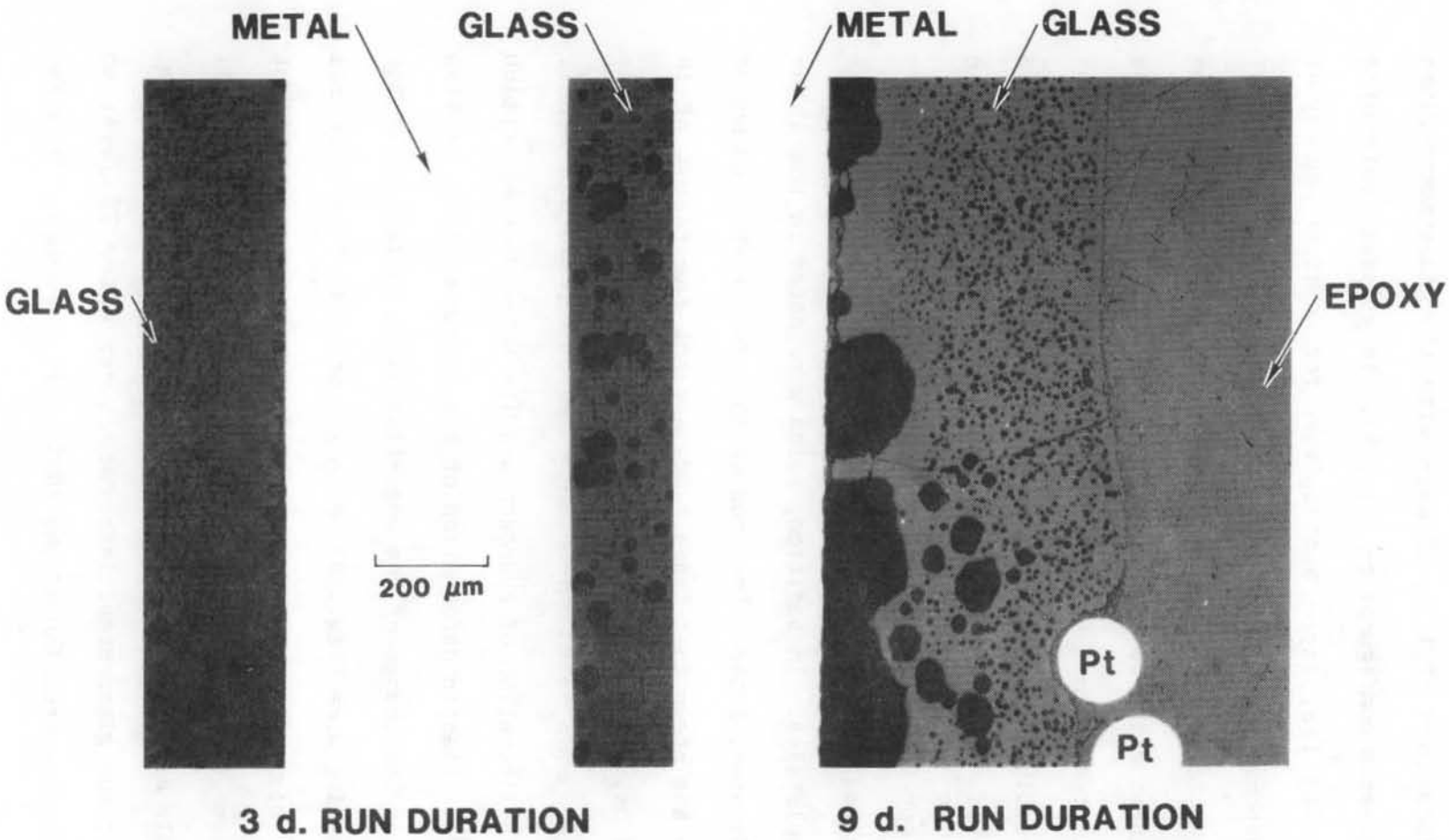

Figure 18. Vapor bubble development in 1095 steel-glass tests at 500°C and 50 MPa (100X photos); glass with 3.0 wt.% dissolved volatiles. The phases present are 1095 steel (metal), glass, platinum binding wire (Pt), and epoxy.

in dramatic contrast to the extensive reactions which occurred at magmatic temperatures.

3. Results of rubble-fluid-metal tests

Ten preliminary rubble-fluid-metal tests were completed for up to 2 weeks duration at temperatures ranging from 650° to 850°C and pressures of 50 MPa. Two day tests with either sieved quartz or alumina particles as the rubble simulant resulted in a fayalite or hercynite reaction rind filling the void space between the rubble and adjacent to the metal wire. Vapor phase transport of the reactive rubble-metal components is a likely mechanism for the rapid buildup of the reaction rind in such a short time. Rhyolite glass rubble-fluid-metal tests at temperatures ranging from 500-750°C and 50 MPa for durations of 2 days have resulted in partial melting of rhyolite at the higher temperatures and extensive alteration of the rhyolite rubble to a quartz-amphibole assemblage at the lower temperatures. All of these reactions would prove to be important to heat transfer across the rubble zone surrounding the heat exchanger, especially in an open system.

4. Summary of technical findings

a. Oxidation is the principal corrosion problem for most of the alloys tested to date; reaction with other magmatic components is limited.

b. Sulfidation of the alloys was not observed in rhyolitic magma, unlike materials tests in basaltic magma.

c. Under magmatic conditions, common austenitic stainless steels show an appreciable penetration of oxygen through grain boundaries.

d. Carbon steels have high reaction rind growth rates in rhyolitic magma.

e. The rate limiting step for reaction rind growth for most materials in rhyolitic magma is mutual volume diffusion of oxygen and metal ions through the oxide rind.

f. Remobilization of sulfur in the 1095 steel is apparently due to the inward sweep of oxygen. Remobilization of sulfur did not occur in other alloys, probably because of their low sulfur content and the limited depth of oxidation into them.

g. Iron-base, nickel-base and cobalt-base superalloys in rhyolitic magma show little grain boundary penetration by oxygen.

h. The presence of 15 wt.% or more chromium in an alloy results in the formation of a protective chromia film.

i. Alloys which are both alumina and chromia formers showed no evidence of grain boundary penetration by oxygen from a rhyolite melt.

j. Refractory metals and alloys are not compatible with rhyolite magma at the high temperatures.

k. Oxidation of metal carbides produces carbon dioxide gas and can lead to high internal gas pressures.

l. Reaction rinds in glass-metal tests are significantly smaller (<10x) than magma-metal rinds.

m. Redox reactions at the glass-metal interface result in the liberation of a gas phase.

n. Voids in the metal were noted in long term glass-metal tests and may be related to hydrous glass-metal interface reactions.

o. Rhyolite glass in glass-metal and rubble-fluid-metal tests exhibits plastic deformation at 500°C and 50 MPa.

p. Rubble-fluid-metal tests at 500-750°C and 50 MPa demonstrate extensive vapor phase transport and exhibit pervasive growth of an intergranular oxide/silicate reaction rind, quartz/amphibole overgrowths on the rhyolite rubble, as well as partial melting.

Conclusions and Recommendations

Although the cost of carbon steels is attractive, they do not have sufficient chemical resistance nor high-temperature strength to be used in the rhyolitic magma environment. Stainless steels and iron-base superalloys may see an application in the hydrothermal environment above the magma zone, but most stainless steels have limited chemical resistance while iron-base superalloys have limited strength at magmatic temperatures, even though their cost is acceptable. Cobalt-base superalloys have excellent chemical resistance to volatile-saturated rhyolitic magma and good strength at 850°C, but they are prohibitively expensive except for special applications involving minor quantities. Nickel-base alloys offer the most promise as candidates for use in rhyolitic environments. Their cost is high,

but they exhibit very good resistance to volatile-saturated rhyolite magma at 850°C and have good strength at these temperatures. Inquiries are being made as to their availability in the required drill stem and casing sizes.

PRESENTATIONS AND PUBLICATIONS

Cygan, R. T., Westrich, H. R., and Weirick, L. J., 1985, Magma-Metal Compatibility: Preliminary results for the Magma Energy Project, EOS, 66, 399.

Gerlach, T. M., Westrich, H. R., Cygan, R. T., and Weirick, L. J., 1985, Characterization and compatibility studies for Magma Energy extraction, Southwestern and Rocky Mountain Division, AAAS, 61st Ann. Mtg., Tucson, AZ, 19-23 March 1985.

Gerlach, T. M., Westrich, H. R., Weirick, L. J., Cygan, R. T., and Stockman, H. W., 1985, Volatile studies at Coso and Long Valley and their application in corrosion investigations in support of the Magma Energy Project, Coso Magma Workshop, Naval Weapons Center, China Lake, CA, 9-10 July 1985.

Westrich, H. R., Cygan R. T., and Weirick, L. J., 1985, Magma-Metal compatibility experiments: Preliminary results for the Magma Energy Program, 1985 International Symposium on Geothermal Energy, 9th Ann. Mtg., Kailua-Kona, HI, 26-30 Aug. 1985.

REFERENCES

American Society for Metals, 1978, Metals Handbook, Ninth Edition. Metals Park, Ohio.

Bacon, C. R., Macdonald, R., Smith, R. L., and Baedecker, P. A., 1981, Pleistocene high-silica rhyolites of the Coso-volcanic field, Inyo County, California, Journal of Geophysical Research, 86, 10223-10241.

Burnham, C. W., 1979, Magmas and hydrothermal fluids, in Geochemistry of Hydrothermal Ore Deposits (Barnes, H. L., editor), John Wiley and Sons, New York, 71-136.

Carmichael, I. S. E., Turner, F. J., and Verhoogen, J., 1974, Igneous Petrology, McGraw-Hill Book Company, New York, 739 p.

Douglass, D. L., 1983, The corrosion of ferritic stainless steels and high-purity Fe-Cr alloys in basaltic lava and simulated magmatic gas, Oxidation of Metals, 20, 161-183.

Douglass, D. L., and Ehrlich, S. A., 1982, The effect of molybdenum plus chromium on the corrosion of iron-nickel, and cobalt-base alloys in basaltic lava and simulated magmatic gas at 1150°C, SAND82-7055, UC-66, Sandia National Laboratories, 75p.

Douglass, D. L. and Healey, J. T., 1979, The corrosion of some pure metals in basaltic lava and simulated magmatic gas at 1150°C, SAND79-1981, Sandia National Laboratories, 72p.

Eichelberger, J. C., and Westrich, H. R., 1981, Magmatic Volatiles in Explosive Rhyolitic Eruptions, Geophysical Research Letters, 8, 757-760.

Gerlach, T. M., and Graeber, E. J., 1985, The volatile budget of Kilauea volcano, Nature, 313, 273-277.

Hardee, H. C., 1984, Shallow magma targets in the western U.S., SAND83-1361, Sandia National Laboratories, 40p.

Hildreth, W., 1979, The Bishop Tuff: Evidence for the origin of compositional zonation in silicic magma chambers, Geological Society of America, Special Paper 180, 43-75.

Nockolds, S. R., Knox, R. W.O'B., and Chinner, G. A., 1978, Petrology for Students, Cambridge University Press, Cambridge, 435 p.

Rundle, J. B. and Whitcomb, J. H., 1984, A model for deformation in Long Valley, California, 1980-1983, Journal of Geophysical Research, 89, 9371-9380.

Rundle, J. B., and Twenty One Others, 1985, Seismic imaging in Long Valley, California, by surface and borehole techniques: An investigation of active tectonics, EOS Transactions, American Geophysical Union, 66, 194-200.

Sanders, C. O., and Ryall, F., 1983, Geometry of magma bodies beneath Long Valley, California, determined from anomalous earthquake signals, Geophysical Research Letters, 10, 690-692.

Stockman, H. W., Westrich, H. R., and Miller, C. D., 1985, EOS Trans. AGU, 66, 385.

Vogel, T. A., Schuraytz, B. C., and Younker, L. W., 1985, Preliminary geothermometry of the conduit to Obsidian Dome based on coexisting ilmenite-magnetite and augite-orthopyroxene, EOS Transactions, American Geophysical Union, 66, 384.

Westrich, H. R., Stockman, H. W., and Taylor, B. E., 1985, Volatile Content of Obsidian Dome and the Inyo Dike, EOS Trans. AGU, 66, 387.

DISTRIBUTION

Lee Younker
Lawrence Livermore National Laboratories
P. O. Box 808
Mail Code L-209
Livermore, CA 94550

Jim Combs
Geothermal Resources International, Inc.
545 Middlefield Road, Suite 200
Menlo Park, CA 94025

Sam Sugine, Jr.
L. A. Dept. of Water and Power
P. O. Box 111
Room 1149
Los Angeles, CA 90051

Harve Waff
Dept. of Geology
University of Oregon
Eugene, OR 97403

Michael P. Ryan
U.S. Dept. of the Interior
Geological Survey
Benston, VA 22092

Tom Henyey
Dept. of Geological Sciences
University of Southern California
Los Angeles, CA 90007

John F. Hermance
Department of Geological Sciences
Brown University
Providence, RI 02912

George A. Kolstad
U.S. Department of Energy
Office of Basic Energy Sciences
Mail Stop J-309
Washington, DC 20585

James Moore
U.S. Geological Survey
345 Middlefiled Road
Menlo Park, CA 94025

L. J. P. Muffler
U.S. Geological Survey
345 Middlefield Road
Menlo Park, CA 94025

Ron Toms
U.S. Department of Energy
Geothermal Hydropower
Technologies Division
Forrestal Bldg., CE 324
1000 Independence Avenue SW
Washington, DC 20585

Mike M. Wright
Earth Science Laboratory
Univ. of Utah Research Inst.
391 Chipeta Way, Suite A
Salt Lake City, UT 84108

James V. Satrape
5113 Leesburg Pike, Suite 700
Falls Church, VA 22041

Dennis T. Trexler
Division of Earth Sciences, UNLV
255 Bell Street, Suite 200
Reno, NV 89503

Mike Sorey
U.S. Geological Survey
345 Middlefield Road, MS 439
Menlo Park, CA 94025

Wm. Christopher Allen
Union Oil Co. of California
Research Department
P. O. Box 76
Brea, CA 92621

David N. Anderson
Geothermal Resources Council
P. O. Box 1350
Davis, CA 95617

John F. Arestad
Santa Fe Geothermal, Inc.
5001 East Commerce Center Drive
Bakersfield, CA 93309

Dr. Carl Austin
Code 266
Geothermal Utilization Div.
Naval Weapons Center
China Lake, CA 93555

John L. Colp, Vice President
Island Science, Inc.
1023 Washington SE
Albuquerque, NM 87108

Bob Decker
Branch of Field Geochemistry and
Petrology
U.S. Geological Survey
345 Middlefield Road
Menlo Park, CA 94025

Mel Friedman
Center for Tectonophysics and
Dept. of Geology
Texas A&M University
College Station, TX 77843

Wilfred Elders
IGPP
Univ. of California
Riverside, CA 92521

Frazer Goff
Los Alamos National Labortories
P.O. Box 1663
Los Alamos, NM 87545

1510 J. W. Nunziato
1513 C. E Hickox
1520 D. J. McCloskey
1524 D. B. Longcope
1530 L. W. Davison
1540 W. C. Luth
1541 H. C. Hardee
1543 T. M. Gerlach (10)
1543 R. T. Cygan
1543 J. C. Eichelberger
1543 M. Reece
1543 H. W. Stockman
1543 H. R. Westrich (20)
1822 K. H. Eckelmeyer
1822 P. F. Hlava
1830 M .J. Davis
1832 J. W. Munford
1841 R. B. Diegle
1841 C. J. Greenholt

1841 L. J. Weirick (5)
6200 V. L. Dugan
6240 R. K. Traeger
6241 J. R. Kelsey
6242 J. C. Dunn (5)
6242 T. Y. Chu
6242 R. D. Jacobson
6242 R. P. Wemple
6242 A. L. Ortega
3141 S. A. Landenberger (5)
3151 W. L. Garner (3)
3154-3 C. H. Dalin (28) for DOE/OSTI
8024 P. W. Dean